

THERMAL AND QUANTUM ANALYSIS OF A STORED STATE
IN A PHOTONIC CRYSTAL CROW STRUCTURE

by

Eduardo M. A. Oliveira, Jr.

A Thesis
Submitted to the Faculty
of the
WORCESTER POLYTECHNIC INSTITUTE
in partial fulfillment of the requirements for the
Degree of Master of Science
in
Electrical and Computer Engineering
by

October 2007

APPROVED:

Professor Brian M. King, Major Advisor

Professor David Cyganski

Professor Sergey N. Makarov

Abstract

Photonic crystals have recently been the subject of studies for use in optical signal processing. In particular, a Coupled Resonator Optical Waveguide (CROW) structure has been considered by M. F. Yanik and S. Fan in “Stopping Light All Optically” for use in a time-varying optical system for the storage of light in order to mitigate the effects of waveguide dispersion. In this thesis, the effects of the thermal field on the state stored in such a structure is studied. Through simulation, this thesis finds that when this structure is constructed of gallium arsenide cylinders in air, loss of the signal was found to be caused by free-carrier absorption, and the decay of the signal dominates over thermal spreading of the optical signal’s spectrum.

Acknowledgements

I would like to thank Professor King for being my advisor, and wish him luck on his future endeavors. Thanks as well to the members of my committee, Professor Cyganski and Professor Makarov, for their time and patience with many delays. Thanks to my wife Amy for putting up with the long nights and poor attention to the “honey-do” list. Finally, if I haven’t mentioned you yet, thank you for reading this.

Contents

List of Figures	vi
List of Tables	viii
1 Introduction	1
1.1 Motivation	1
1.2 Applications	2
1.3 Related Topics	4
2 Background	6
2.1 Photonic Crystals	6
2.2 Waveguides	12
2.3 Coupled Resonator Optical Waveguides	17
2.4 Dispersion in Photonic Crystals	20
2.5 Time Dynamic Waveguides	23
2.6 Yanik and Fan Structure	25
2.7 Quantum Mechanics in Dielectric Media	27
3 Electromagnetic Analysis of the Yanik and Fan Structure	30
3.1 Modes and Band Diagrams of the Simple Yanik and Fan Structure	31
3.2 Modes and Band Diagrams of the Realistic Yanik and Fan Structure	35
3.3 Density of States for the Simple Yanik and Fan Structure	38
3.4 DOS in Realistic Yanik and Fan Structure	39
3.5 Outcome of Electromagnetic Analysis	42
4 Application of Quantum Analysis to CROWs	43
4.1 Quantum in Crystalline Solids	43
4.1.1 Dipole Approximation	44
4.2 Phonons in Crystalline Solids	44
4.3 Yanik and Fan Structure	45
4.4 Adiabatic Tuning of the Basic Structure	46
4.5 Conditions for Maintaining Adiabatic Transitions	48
4.6 Other Quantum Effects	48

5	Thermal Spreading	50
5.1	Classical Thermal Losses	50
5.2	Quantum Thermal Losses	53
5.3	Methodology for Modeling Thermal Interaction	54
5.4	Implementation of Algorithm	60
5.5	Results from Simulation of Yanik and Fan structure	61
6	Conclusions	66
A	Thermal Simulation MATLAB Script	69
B	Example MPB Script: Realistic Yanik and Fan Structure in Open State	81
	Bibliography	84

List of Figures

2.1	3D Brillouin Zone of a Face Centered Cubic Lattice	10
2.2	2D Brillouin Zone of a Square Lattice	11
2.3	Bragg Mirror Structure	12
2.4	Bands of a Bragg Mirror, unwrapped (left) and wrapped (right)	13
2.5	Propagation Velocity, First Three Bands of Bragg Mirror	14
2.6	TE (Left) and TM (Right) Modes of a 2D Photonic Crystal	15
2.7	2D Photonic Crystal Lattice of Cylindrical Rods	15
2.8	Waveguide Channel in a Photonic Crystal	16
2.9	Single Photonic Crystal Resonator in a 2D Square Lattice	17
2.10	Normalized Electric Field Mode of a Single Resonator in a Square Lattice 2D Photonic Crystal versus x and y Normalized to the Lattice Constant . .	18
2.11	Coupled-Resonator Optical Waveguide (CROW) Structure	19
2.12	Propagating Mode in a CROW	20
2.13	Propagation Velocity within a CROW	21
2.14	Propagating Frequencies of a CROW	22
2.15	Dispersion Due to Nonlinear Phase: The effect of a dispersive system on the square wave is to shift the phase of the frequencies that make it up. This can have drastic effects, as seen in the upper-right figure.	22
2.16	Modes of a Parallel Plate Waveguide	23
2.17	Effect on First Mode Due to Time Varying Waveguide	24
2.18	Yanik and Fan structure	25
2.19	Propagating Mode in a CROW: Top-down view	26
3.1	Dispersion Bands for Simple Yanik and Fan Structure: The figure on the right shows a zoomed in version of the guided bands	31
3.2	Comparison of Bands for Simple Yanik and Fan Structure in the Propagating State (Left) and Storage State (Right)	32
3.3	The Propagating Mode of the Simple Yanik and Fan Structure (Normalized Electric Field Amplitude, x and y Displacement Normalized to the Lattice Constant)	33
3.4	The Stored Mode of the Simple Yanik and Fan Structure (Normalized Electric Field Amplitude, x and y Displacement Normalized to the Lattice Constant)	34
3.5	Bands for the Realistic Yanik and Fan Structure in the Storage State	35

3.6	Bands in the Band Gap of the Realistic Yanik and Fan Structure in the Propagating State	36
3.7	Bands for the Realistic Yanik and Fan Structure in the Storage State	36
3.8	Comparison of Bands in the Band Gap of the Realistic Yanik and Fan Structure in the Storage State (Left) and Propagating State (Right)	37
3.9	Density of States in the Band Gap of the Simple Yanik and Fan Structure, Histogram Bin Size = $5.9375 \cdot 10^{-7}$	38
3.10	Density of States in the Realistic Yanik and Fan Structure, Histogram Bin Size = $5.9375 \cdot 10^{-7}$	39
3.11	Density of States for the Realistic Yanik and Fan Structure in the Storage State, Histogram Bin Size = $5.9375 \cdot 10^{-7}$	40
3.12	Density of States for the Realistic Yanik and Fan Structure in the “Pass Through” State, Histogram Bin Size = $5.9375 \cdot 10^{-7}$	40
3.13	Density of States for the Realistic Yanik and Fan Structure in the Storage State, Histogram Bin Size = $5.9375 \cdot 10^{-7}$	41
3.14	Density of States for the Realistic Yanik and Fan Structure in the “Pass Through” State, Histogram Bin Size = $5.9375 \cdot 10^{-7}$	41
4.1	DOS of a 2D Square lattice, Histogram Bin Size = $5.9375 \cdot 10^{-6}$ in Normalized Frequency	46
4.2	DOS of a 2D Square lattice with defect, Histogram Bin Size = $5.9375 \cdot 10^{-6}$ in Normalized Frequency	47
5.1	Carrier Distribution in Gallium Arsenide at 300K	62
5.2	Thermal Interaction with the Compressed State.	63
5.3	Deterioration of Signal in Stored State, Including Effects Due to Thermal Field	64
5.4	Percent Difference between Signal with Thermal Spreading and without Thermal Spreading	64

List of Tables

2.1	Coupling Coefficients of a CROW	19
5.1	Material Properties for Gallium Arsenide	59

Chapter 1

Introduction

Photonic crystals are structures in which the refractive index varies periodically. These structures are known for their important properties, the first of which is a band-gap, a range of frequencies which are not allowed to propagate in the material. Another important property is slow light propagation for frequencies near the edge of the band gap. These properties can be utilized in a wide array of applications which motivate further study.

A variety of uses arise when one is able to vary the properties of these structures with time. These applications include optical switching, optical storage, signal processing, and optical computing. The interaction of light with these structure create new opportunities in each of these fields.

This paper studies thermal and quantum effects in a time varying photonic crystal wave guide structure proposed in [35] for use in storing an optical signal. Special attention is given to the study of the interaction between the stored state and the thermal field.

1.1 Motivation

Photonic crystal structures are growing in popularity as a tool for manipulating light signals. The most simple and common uses are waveguiding light in photonic crystal fibers and as an optical cavity for semiconductor lasers. New uses for photonic crystal structures are emerging, especially when nonlinear materials are added as a component of the

structure [36, 35, 38].

The slow light property of photonic crystals is due to the dispersion relationship having nearly zero slope near the band edge. Because refractive index can be defined as the ratio of the speed of light to the phase velocity, the situation can be interpreted as propagating modes near the band edge experiencing a high effective refractive index. Slow light can result in significant enhancement of interaction effects between the material and the field. For example, in nonlinear materials, more effective optical mixers can be made, as well as enhanced frequency conversion can be achieved. Also, interactions between the quantum states of the dielectric and the electric field can be enhanced [21].

If it can be shown that the quantum state can be maintained within a light storage structure, the structure will have broad applications within fields such as quantum computing. The system could be used as a quantum state delay line or a quantum state latch. Such quantum state storage devices are highly sought after for quantum computing for use as memory.

1.2 Applications

Due to the slow light property of photonic crystals, they can be utilized for optical storage. Optical storage can be achieved by varying the phase delay of a system. Also, if the group velocity can be slowed dramatically, optical storage is obtained because the slow group velocity prevents the signal from propagating through the material before the required storage time. In a photonic crystal system, group velocity of propagating fields can be changed by perturbation of the material properties, mechanically changing the dimensions of the photonic crystal, or by Doppler shifting the field toward or away from the band edge. Storage of an analog signal such as the result of optical Fourier transform or an optical holographic search is possible. Digital optical data can also be stored holographically within a photonic crystal system. A photonic crystal system can also act as a delay element.

New designs including optical gates and transistors using photonic crystals will lead to the possibility of optical computing [36, 35, 38]. Optical computing systems have an advantage over conventional systems in that certain tasks can be highly parallelized. Because of

this, they can be used to test multiple cases simultaneously [32]. Practical optical storage will be an important key to such optical processing systems.

Photonic crystals are already showing promise for use in optical computing, by allowing optical AND gates to be built with 20 dB of power gain [38]. In reference [38], photonic crystals are used to construct an interferometer with the output controlled by a non-linear element. The non-linear effect is enhanced by the field localization within the photonic crystal, resulting in an AND gate with 20 dB changes in the output when the input thresholds are crossed by just a few dB. With the development of the remaining gates, optical digital “circuits” can be designed, and all-optical computing can become a reality.

In addition to optical computing using classical waves, quantum optical computing has additional advantages. When using a quantum computer, the system can be initialized to a mixed state of all the possible outcomes of the problem. From that point, it takes the same time to check for every possible outcome as it does for a single possibility. The quantum computer processes the initial state via quantum interference. Because of this, it is desirable to have a tunable quantum optical delay in order to have optically-controlled quantum interference for quantum computing.

Because photons very rarely directly interact with each other, most photon-photon interactions are actually photon-matter-photon interactions. As a result, materials must be developed that enhance and guide photons in dielectric media in order to perform quantum optical tasks. The next chapter reviews the fundamentals of the interaction between light and matter, and describes useful photonic crystal structures. This will include a system for the delay and storage of light as put forth by Yanik and Fan in reference [35].

1.3 Related Topics

This thesis will endeavor to quantify the loss of a state in time in a photonic crystal storage structure. Similar calculations have been made by others in order to study lasers and infrared sensors. This section outlines some of the work in this area.

In [2], free carrier absorption in silicon relating its loss tangent was empirically examined. Free-carrier absorption was found to be the main absorption effect for wavelengths in the microwave into the far infrared range for silicon.

The problem of absorption arises during the study of lasers which includes effects such as thermal broadening of the spectral line width. For example, in [31], a model was derived for free-carrier absorption from first principles using second order perturbation theory. This study included acoustic, optical phonons, deformation potential phonons, piezoelectric acoustic phonons and charged impurities. Also shown in [31] is how the square of wavelength relationship for losses prediction of Drude conductivity fails to predict free-carrier absorption for certain wavelengths.

In addition to lasers, another area in which the problem of free-carrier absorption occurs is in infrared detectors [16]. By modeling heavily doped quantum well structures, the paper accounted for many-body effects, intersubband absorption, and free-carrier absorption. The method outlined in [31] is useful for analyzing structures in which free carrier absorption is the primary loss mechanism. The paper dedicates attention to semiconductors with the multiple interacting energy valleys such as indirect band gap materials such as silicon and germanium.

Yet another paper studied the use of Monte Carlo simulations to predict carrier dynamics [13]. The approach used accounts for DC electric fields and carrier-carrier interactions. The paper compared Monte Carlo results for heavily doped silicon to experimental results, and found that acoustic phonon scattering and impurity scattering were the main loss mechanisms in most of the samples.

In [10], a method for measuring bulk lifetime and surface recombination was described. The theoretical efficiency of silicon solar cells was discussed in [30]. In [24], Schroder et al. studied photo detection hampered by infrared signal absorption in heavily doped silicon,

using the Drude model. The relationship between carrier heating due to stimulated emission and free-carrier absorption in semiconductor lasers was undertaken in [33].

Fronen et al. studied intensity fluctuation and increased spectral width due to changes in the absorption coefficient and fluctuations in free-carrier concentration [9]. Both these potential sources predict similar levels of $1/f$ noise, and each matched experimental results.

Line width rebroadening due to spatial hole burning, carrier density distribution, mode partition, and spontaneous emission noise was studied in [28]. In [7], the authors studied spectrum effects in semiconductor lasers, specifically, shift of the peak and broadening due to gain, band filling and bands shrinkage. A lens design for a high efficiency laser cavity was discussed in [17].

The latest research into photonic crystals shows much promise in the optical signal processing and optical computing fields. In this chapter we have discussed just a few aspects of the research in this field. The next chapter further discusses the background information necessary for the study of photonic crystals.

Chapter 2

Background

In order to investigate the optical properties of photonic crystals, one must first review how the wave equation arises from Maxwell's equations, and how the periodicity of photonic crystals leads to Bloch modes. These theories explain concepts such as the dispersion diagram, group velocity, and density of states (DOS). How photonic crystals can be used as waveguides, resonators, and coupled resonator optical waveguides (CROWs) is also discussed in this chapter.

2.1 Photonic Crystals

To achieve a good foundation for the study of photonic crystals, one should first review wave propagation due to Maxwell's equations. Assuming that there are no sources (current or charge density) in the area of interest (i.e. they are infinitely far away), and that the permittivity of the material is not dependent on electric field intensity and frequency, are as follows:

$$\nabla \cdot \mathbf{B}(\mathbf{r}, t) = 0 \quad (2.1)$$

$$\nabla \times \mathbf{E}(\mathbf{r}, t) + \frac{1}{c} \frac{\partial \mathbf{B}(\mathbf{r}, t)}{\partial t} = 0 \quad (2.2)$$

$$\nabla \cdot \mathbf{D}(\mathbf{r}, t) = 0 \quad (2.3)$$

$$\nabla \times \mathbf{H}(\mathbf{r}, t) - \frac{1}{c} \frac{\partial \mathbf{D}(\mathbf{r}, t)}{\partial t} = 0 \quad (2.4)$$

Where c is the speed of light in a vacuum, the displacement field \mathbf{D} is defined in terms of the electric field \mathbf{E} as:

$$\mathbf{D}(\mathbf{r}, t) = \epsilon(\mathbf{r})\mathbf{E}(\mathbf{r}, t) \quad (2.5)$$

where $\epsilon(\mathbf{r})$ is the permittivity of the medium, and the magnetic induction field \mathbf{B} is defined in terms of the magnetic field \mathbf{H} as:

$$\mathbf{B}(\mathbf{r}, t) = \mu(\mathbf{r})\mathbf{H}(\mathbf{r}, t) \quad (2.6)$$

where $\mu(\mathbf{r})$ is the permeability of the medium. For absorptive materials, complex permittivity and permeability can be used, while for anisotropic materials, the permittivity and permeability are tensors of rank 2.

The time-harmonic solution can be found, using complex exponential Fourier series to solve the time dependent part of the equations, and when Equations 2.5 and 2.6 are substituted into Equations 2.2 and 2.4, the result is

$$\nabla \times \mathbf{E}(\mathbf{r}) + \frac{i\omega}{c}\mathbf{H}(\mathbf{r}) = 0 \quad (2.7)$$

$$\nabla \times \mathbf{H}(\mathbf{r}) - \frac{i\omega}{c}\epsilon(\mathbf{r})\mathbf{E}(\mathbf{r}) = 0 \quad (2.8)$$

When the inverse of $\epsilon(\mathbf{r})$ multiplies both sides, Equation 2.8 is substituted into Equation 2.7, and the inverse of $\mu(\mathbf{r})$ multiplies both sides, the result is

$$[\mu(\mathbf{r})]^{-1}\nabla \times [[\epsilon(\mathbf{r})]^{-1}\nabla \times \mathbf{H}(\mathbf{r})] = \left(\frac{\omega}{c}\right)^2 \mathbf{H}(\mathbf{r}) \quad (2.9)$$

This is an eigenvalue problem that has the property that the operator on the left is Hermitian, and therefore has real eigenvalues and orthogonal eigenfunctions. If $[\mu(\mathbf{r})]^{-1}$ is positive definite the eigenvalues can be shown to be positive, the variational principle can be applied in order to find the eigenfunctions[14]. This is true, for example, if $\mu(\mathbf{r})$ is a positive constant, which is the case for dielectric and other non-magnetic materials.

If the index of the material is not spatially varying, one notes that the ϵ^{-1} can be brought through the curl to the left, and the magnetic field eigenfunctions are plane waves. Each of these plane waves can be written in the form $e^{i\mathbf{k}\cdot\mathbf{r}}$ where \mathbf{k} is the wavevector defining the direction and wavelength of the plane wave. The momentum of the wave is proportional to the \mathbf{k} vector, and the proportionality constant is \hbar .

The result of this analysis of the wave equation is that $\frac{k^2}{\epsilon_r} = \left(\frac{\omega}{c}\right)^2$. This equation relates the length of the wavevector \mathbf{k} (also known as the wavenumber, k) to the frequency ω via the phase velocity of the plane waves $\frac{c}{\sqrt{\epsilon_r \mu_r}}$ [22]. If there is a single plane interface between two materials, the solution on each side of the boundary has eigenfunctions that are plane waves and boundary conditions can be matched at the interface. This procedure can be applied when the field reflects off of the multiple interfaces. In such a case, the waves will either constructively or destructively interfere, and only those which have a round trip which remains in phase with itself will have a non-zero contribution.

Because plane waves are eigenfunctions of the curl operator, it is generally useful to describe the magnetic field in terms of plane waves in the form of a Fourier series expansion.

The scaling properties of Maxwell's equations will prove helpful in the study of photonic crystals as well. It can be shown that Maxwell's equations are scalable in distance and relative permittivity; that is, if there is a solution to Maxwell's equations for one spatial scale or relative permittivity, the solution at another spatial scale or relative permittivity is simply a scaled version of the original. The only change is that the eigenvalue associated with each of the original eigenfunctions is scaled by a constant [14].

One use of distance scalability is that if one wants to design a system for optical frequencies but cannot maintain the tolerances for those small spatial distances, one can instead make a macroscopic model, and test this model with fields that have the wavelength scaled by the same factor.

Another useful property is that Maxwell's equations are reversible in time. One example of the time reversal property of Maxwell's equations is that a spherical wave expanding out from a point source implies that a solution exists where spherical waves are converging on a point.

Because Maxwell's equations are fully scalable, distances inside a photonic crystals can be normalized in terms of the lattice constant a , and the \mathbf{k} vectors can be normalized by a scale factor of $\frac{2\pi}{a}$. Velocities can naturally be normalized to c . As a result of these scale factors, it is convenient to normalize frequency by a scaling factor of $\frac{a}{2\pi c}$.

Photonic crystals are periodic structures of materials with two (or more) indices of refraction. When one solves for the fields in such a structure, one finds that if the permittivity

is periodic in space, the eigenfunctions must have a form that consists of the product of a wave which has the same periodicity as the lattice and a plane wave corresponding to a valid \mathbf{k} vector. This is known as a Bloch wave. The propagating electric and magnetic fields within the photonic crystals are therefore Bloch waves in the limit of infinitely-long periodic structures.

Photonic crystals are also possible in two and three dimensions. Of course, in each dimension that the dielectric structure is periodic, the electric and magnetic fields must also be periodic. For each direction of periodicity, there is a lattice vector that describes a direction in the lattice. The length of the lattice vectors are known as the lattice constants. Each lattice constant has a length equal to the spatial period of the lattice. Often, the lattice is symmetric and only one lattice constant is necessary. The lattice is spanned by the lattice vectors in the same way that any other space is spanned by vectors. The lattice constant a may be considered to be the magnitude of lattice vector. If the lattice is symmetric, then one constant can describe the periodicity of the lattice.

If one were to perform a Fourier series decomposition of $\epsilon(\mathbf{r})^{-1}$, one would find that there exists reciprocal lattice vectors which are the \mathbf{K} vectors, which are the Fourier transform of the \mathbf{k} vectors which have the property that $e^{i\mathbf{K}\cdot\mathbf{R}} = 1$. This set of primitive vectors spans what is known as the Brillouin zone, where \mathbf{R} is the reciprocal of the spatial displacement \mathbf{r} .

The Brillouin zone can also be thought of in the following way: if there is a point in the lattice with an epsilon $\epsilon(\mathbf{r})$, there are vectors \mathbf{k} such that the value of epsilon is repeated for integral multiples of \mathbf{k} ; that is, $\epsilon(\mathbf{r}) = \epsilon(\mathbf{r} + m\mathbf{k})$, where m is an integer. This means the entire lattice can be regenerated from a single period of the lattice by translating it by \mathbf{k} scaled by an integer. This single lattice period is known as the first Brillouin zone.

By utilizing the rotational and reflection symmetry within the Brillouin zone, one can further reduce the unit cell. The unit cell that is derived this way is known as the irreducible Brillouin zone. The irreducible Brillouin zone has the property that any point that is in it can not be reached by using the available symmetry, translation, or rotation, i.e. all the symmetries have been exploited to arrive at the irreducible Brillouin zone. Continuity and symmetry of the electric and magnetic fields is used to generate the complete wave solutions

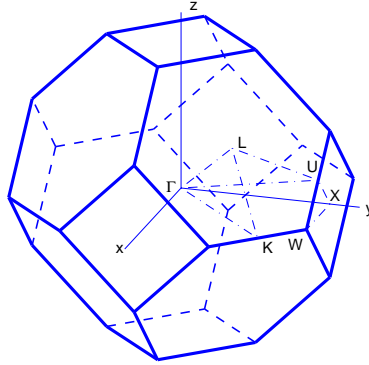


Figure 2.1: 3D Brillouin Zone of a Face Centered Cubic Lattice

from the irreducible Brillouin zone. Figure 2.1 shows the Brillouin zone of a face centered cubic lattice.

In reference [14], Joannopoulos describes an intuitive way of describing the Brillouin zone: If one bisects the distance between the nearest neighbor lattice points, the region bounded by these lines (or planes in the case of a 3 dimensional lattice) is the Brillouin zone. Figure 2.2 illustrates this relationship in the case of the square lattice. Note that the reciprocal lattice in this case is also a square lattice. The irreducible Brillouin zone can be identified as one of the triangles in the figure created by the segments connecting the lattice points. The standard choice in case of the square lattice is the triangle bordered on the bottom by the k_x axis, whose vertices are Γ , at the origin, $X = (\frac{\pi}{a}, 0)$ on the k_x axis, and $M = (\frac{\pi}{a}, \frac{\pi}{a})$ at the remaining vertex of the triangle, as indicated in Figure 2.2. The nomenclature for these points originates from x-ray diffraction crystallography.

This periodicity of the field solutions for photonic crystals lead to band splitting, which causes the important properties such as enhanced transmission or the band-gap – a band of frequencies for which no transmission occurs with only an evanescent field extending into

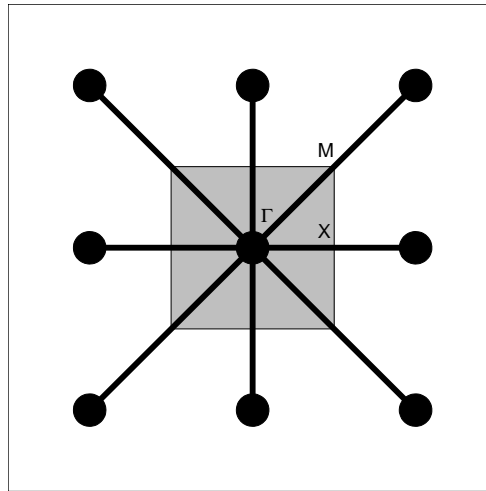


Figure 2.2: 2D Brillouin Zone of a Square Lattice

photonic crystal. A simple example of a photonic crystal with which to illustrate this point is the Bragg mirror. A Bragg mirror is a photonic crystal that is periodic in one dimension, such as the structure shown in Figure 2.3. In this example, the lattice is one of air and a dielectric with index of refraction $n = 3.6$ (such as GaAs) with thicknesses $a/2$ and $a/2n$ where a is the lattice constant. Figure 2.4 shows the dispersion relationship for this Bragg mirror.

Because of the periodicity of the lattice, any band that exists for a high spatial frequency has a copy at a lower spatial frequency with a k vector that is of length nk_o where n is an integer. Therefore all the bands appear within the first Brillouin zone, and one can “fold” the longer k vector frequency results. Typically, the bands are shown folded over on the repetitions of the reduced lattice interval shown on the Figure 2.4 on the right. If one were to draw tangents out from the low frequency bands, a diamond pattern would form on the dispersion diagram. Away from the band edges, the bands follow this diamond pattern made up of what are known as the “light lines” for the dispersion diagram. However, at the edges of the irreducible Brillouin zone, the bands repel each other, leading to what is known

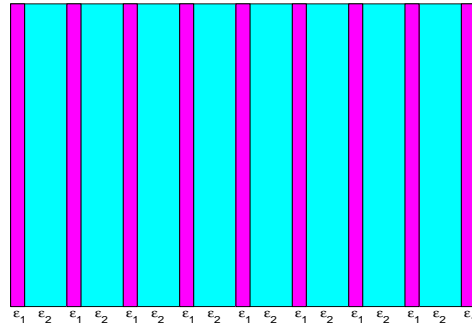


Figure 2.3: Bragg Mirror Structure

as band splitting [21]. This splitting bends the bands toward the horizontal, thus slowing the propagation velocity while opening up band gaps where the bands would have crossed. In reference [21], Sakoda shows analytically that when the first two terms of the Fourier series of a periodic dielectric are taken, the zero-order term sets the light line, while the term associated with the fundamental spatial frequency leads to band splitting proportional to the square root of the magnitude of that term. The splitting can be interpreted as “mixing” of the modes above and below where the light lines cross on the dispersion diagram at $k = \frac{\pi c}{a}$ [21].

Thus far the electromagnetic properties of photonic crystals have been discussed. The next chapter will show that when defects are added, photonic crystals can be used as resonators and waveguides.

2.2 Waveguides

To better understand waveguiding in the context of photonic crystals, the properties and principles of waveguides should first be reviewed. A waveguide is a device for transmitting waves, such as light waves, most often via multiple reflections, to direct light from a source to the desired destination. Very often, this is accomplished via total internal reflections inside a dielectric that is encased in another dielectric of lower index, as in the case of an

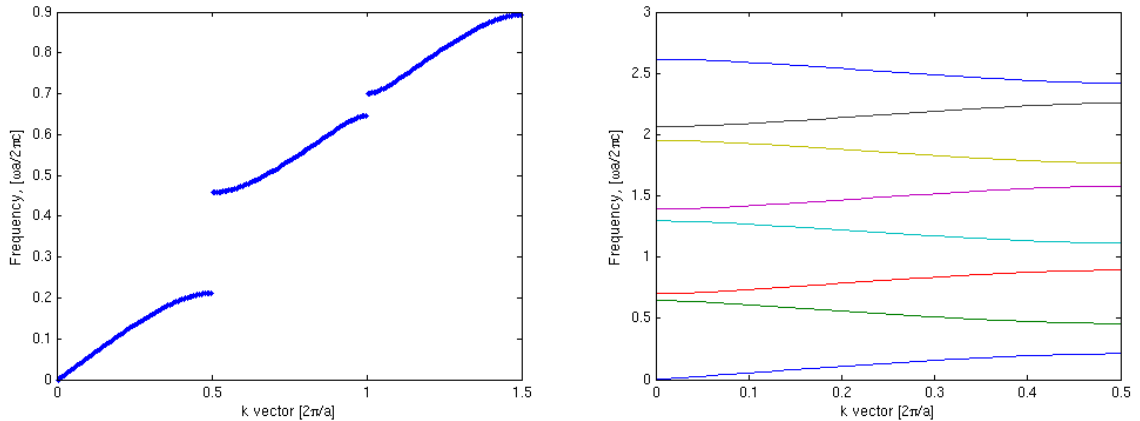


Figure 2.4: Bands of a Bragg Mirror, unwrapped (left) and wrapped (right)

optical fiber. If a transverse electromagnetic wave impinges upon an interface with angle θ , it will be reflected with angle θ and continue to the other interface where it will be reflected again and travel down the waveguide. If the result is that there are only two distinct plane waves traveling down the waveguide, one with a positive angle θ with respect to the axis along the waveguide and one with a negative angle θ with respect to this axis, the field is said to be a mode of the waveguide. The modes each satisfy different bouncing angles. The transverse component of the wavevector is quantized, and the component of the wavevector in the direction of propagation is known as the propagation constant for the mode. The total electric field propagating in the waveguide can be written as a sum of the modes.

Each band on the dispersion diagram represents a mode of the system. In many common cases, the modes of a waveguide are orthogonal to each other. The set of eigenmodes of a waveguide is incomplete as compared to the modes of a vacuum. A mode in one system couples to one in another system to the extent that one mode projects onto the other. This also holds for coupling between the vacuum field and the waveguide modes. The energy that is orthogonal to all the waveguide modes is not coupled and is reflected.

As one can see from Figures 2.4 and 2.5, there are band gaps, where frequencies have no modes in which to propagate. One can also observe from these figures that near the

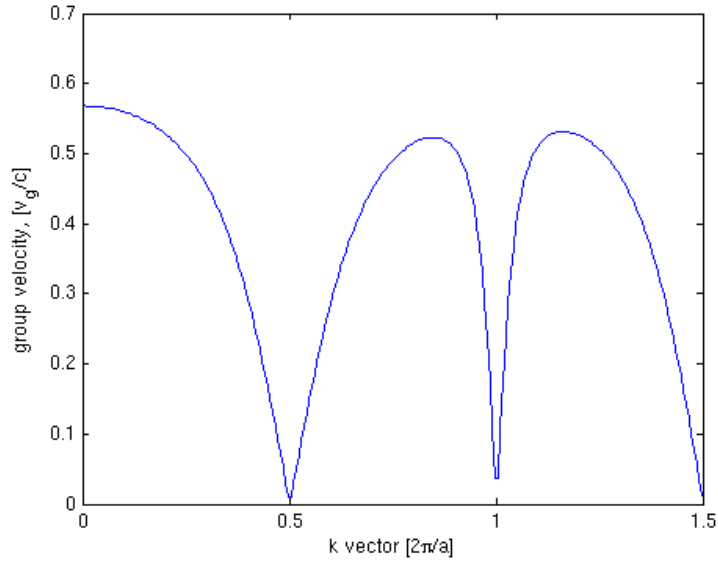


Figure 2.5: Propagation Velocity, First Three Bands of Bragg Mirror

band edges light propagates slowly because the slope of the dispersion diagram is the group velocity of the mode at that point. Figure 2.5 shows the group velocity for the first three bands versus k vector in the propagation direction, and further demonstrates the slow light condition at the band edges. Because refractive index is defined as the ratio of the speed of light to the propagation velocity, high effective index is possible for propagating modes.

Complete band gaps in all polarizations and directions become increasingly difficult to create as one attempts to construct photonic crystals in higher dimensions. It is often the case, for example, to have a 2D photonic crystal that has a band gap for all directions of the TM mode at around $0.3 \frac{a}{2\pi c}$, but the band gap for the TE mode is for a completely different set of frequencies near $0.8 \frac{a}{2\pi c}$ as seen in Figure 2.6 for the case of cylindrical rods on a square lattice that is depicted in Figure 2.7. In fact, for certain choices of rod diameter, the TE band gap disappears completely. In the dispersion diagrams of the 2D photonic crystals in this paper, the k vector is indexed rather than its value given. The indices represent the high symmetry points around the edges of the irreducible Brillouin zone, where index “T” represents the k vector with k_x and k_y equal to zero, index “X” corresponds to a k

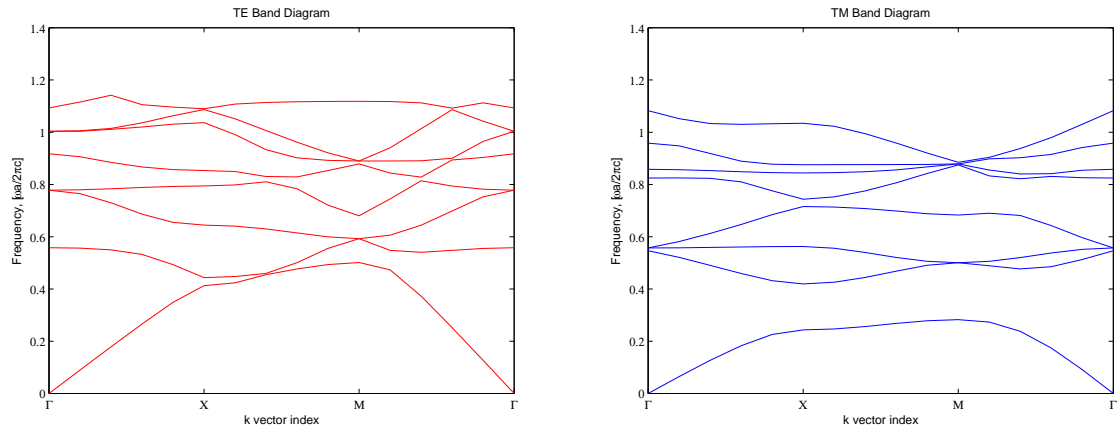


Figure 2.6: TE (Left) and TM (Right) Modes of a 2D Photonic Crystal

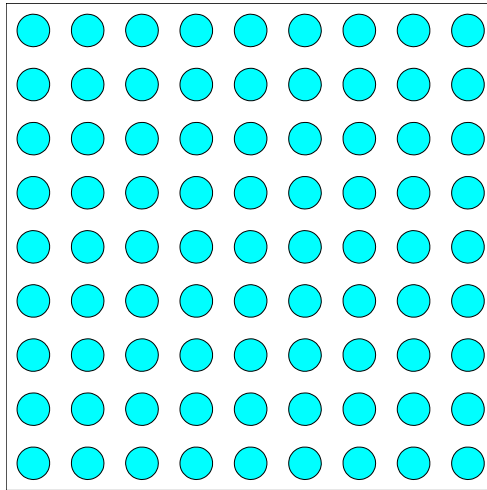


Figure 2.7: 2D Photonic Crystal Lattice of Cylindrical Rods

vector with k_x equal to $0.5/a$ and k_y equal to zero, and index “M” corresponds to a k vector with k_x and k_y equal to $0.5/a$ as was seen in Figure 2.2. The differing band gaps for the TE and TM modes can sometimes lead to a possible benefit when one wants to separate polarizations, which is often the case in laser cavities, for example. Still, it is often useful to have a complete band gap and in these cases the design is more difficult and the set of photonic crystals that have a complete band gap become a smaller portion of the set of possible configurations of the microstructure of the photonic crystal.

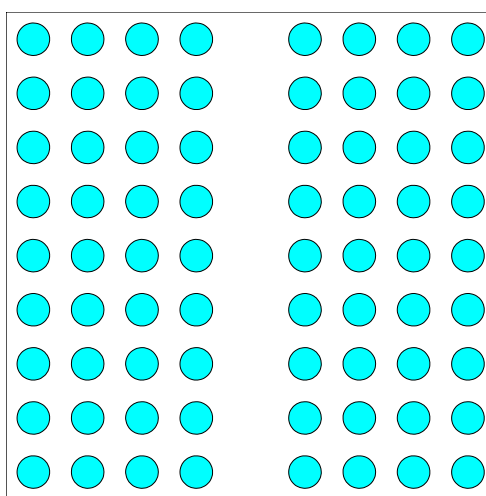


Figure 2.8: Waveguide Channel in a Photonic Crystal

One of the main applications for photonic crystals today is optical waveguides. The waveguide is generally realized by introducing a linear defect, for example, eliminating one or more rows of the photonic crystal as seen in Figure 2.8. This results in a case analogous to the dielectric slab waveguide, with the exception that the wave may be propagating in a medium that has higher or lower effective index than the reflecting “surfaces” of the photonic crystal waveguide. In the standard waveguide, the reflecting surfaces must have lower index than the waveguide channel.

Another application of photonic crystals is as a resonator. A resonator may be realized

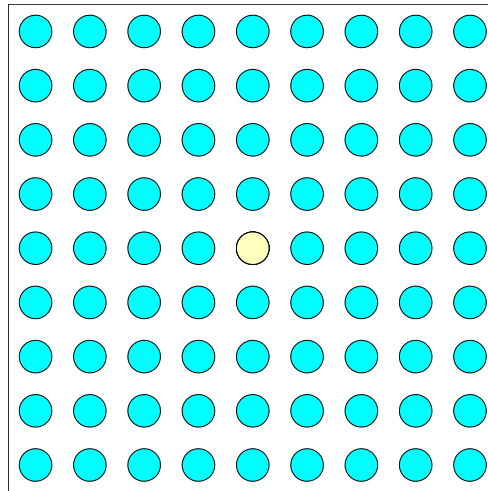


Figure 2.9: Single Photonic Crystal Resonator in a 2D Square Lattice

by adding a single defect into the periodic structure. One can imagine that, if a defect were surrounded by a perfect photonic crystal as depicted in Figure 2.9, a mode could exist inside the defect that would be forbidden in the rest of the structure. This would comprise a photonic crystal resonator. Figure 2.10 shows the mode that can be sustained inside the defect of such a resonator made up of a square lattice of dielectric rods of radius $0.2a$ where the defect has an index of 2.8. This mode is localized, and can only be reached by evanescent coupling to the outside of the photonic crystal or to another defect within the photonic crystal, or by other loss mechanisms such as coupling to the thermal modes of the photonic crystal and scattering off imperfect surfaces. Photonic Crystal resonators have increasingly been used to form the resonator cavities in semiconductor lasers.

2.3 Coupled Resonator Optical Waveguides

The reader may note that Figure 2.10 also shows that the mode has energy in the nearby rods. This is the evanescent field decaying as it penetrates into the photonic crystal. If one

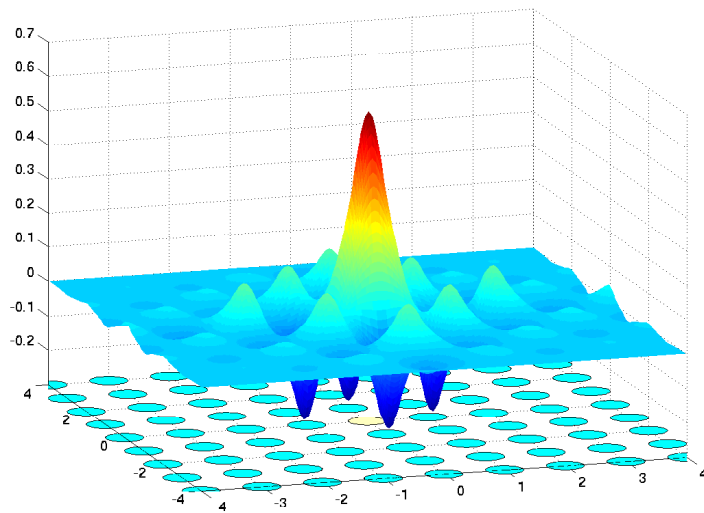


Figure 2.10: Normalized Electric Field Mode of a Single Resonator in a Square Lattice 2D Photonic Crystal versus x and y Normalized to the Lattice Constant

Spacing [a]	Coupling Coefficient
2	0.0011946
3	0.00052748
4	0.00023951
5	0.00012298

Table 2.1: Coupling Coefficients of a CROW

of these rods is also replaced by a defect, the evanescent field of this mode will couple to this defect. This coupling process could be repeated again and again if several defects are placed at regular intervals. The result is a mode that propagates between the resonator defects, which can exist in what was the band-gap of the bulk material [37]. This structure is known as the Coupled-Resonator Optical Waveguide (CROW). An example of such a structure is shown in Figure 2.11. MIT Photonic Bands (MPB) software [15] and MATLAB were used to calculate the coupling coefficients for a square lattice of cylindrical rods of index of 3.6 with defects of index 2.8 spaced at two to five lattice constants apart as shown in Table 2.1. Note that the coupling coefficients decrease exponentially as a function of distance, as would be expected for evanescent coupling.

The mode shown in Figure 2.12 may propagate extremely slowly because the coupling of the modes is inversely proportional to the propagation velocity of the mode. Figure 2.13 shows the propagation velocity as a function of k vector for the given mode. Notice that

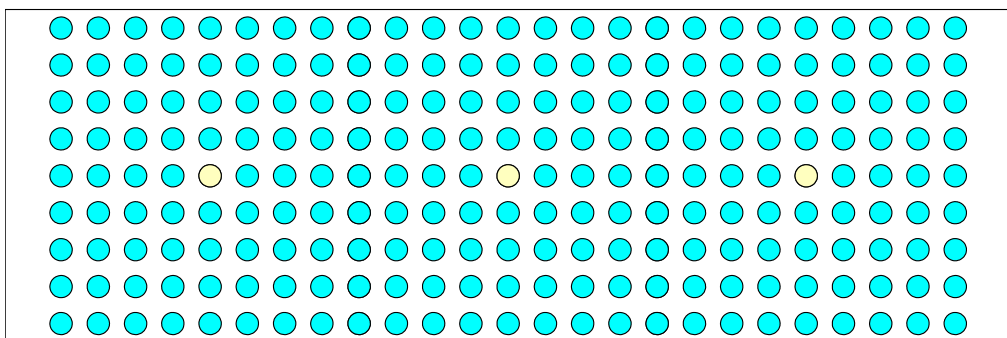


Figure 2.11: Coupled-Resonator Optical Waveguide (CROW) Structure

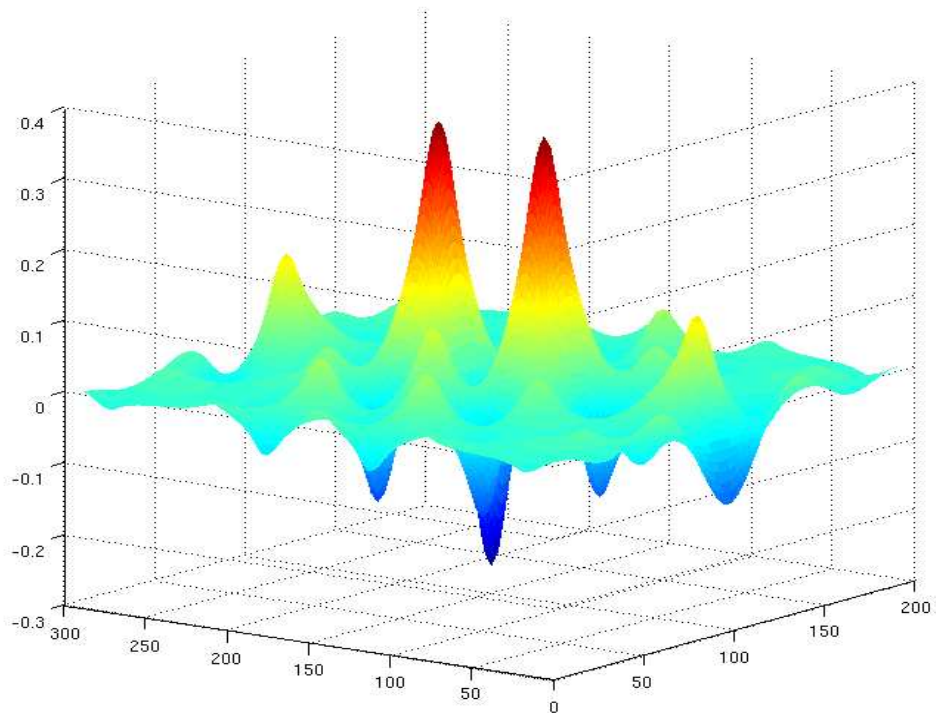


Figure 2.12: Propagating Mode in a CROW: The energy from the mode transfers from one defect to the next as it propagates along the waveguide. The scale along the bottom edges is in lattice constants.

as the k vector approaches $\frac{2\pi}{a}$ the group velocity drops to $0.01c$. Because of the symmetry of the evanescent field, it is straightforward to deduce that the waveguide can contain 90 degree bends without reflection for all frequencies carried by the mode. The propagating mode for this waveguide is depicted in Figure 2.12, and the bands associated with this mode can be found in Figure 2.14.

2.4 Dispersion in Photonic Crystals

With the extremely slow modes that exist in the CROW waveguide, one may consider using a CROW as a delay element. In general, however, there is a problem that arises.

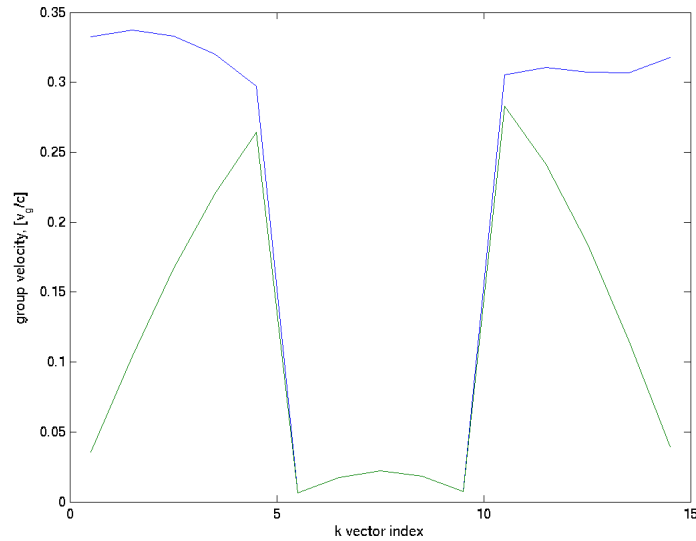


Figure 2.13: Propagation Velocity of a CROW: The propagation velocity decreases to nearly zero at the band edges

Because the group velocity is the slope of the band on the dispersion diagram, the curvature of these bands (such as in Figure 2.5) means that different frequencies will be traveling at different speeds. Therefore, dispersion in the CROW is quite high for signals of moderate bandwidth because the propagation velocities in a single band of a CROW can vary by many orders of magnitude for different frequencies. This causes drastic dispersion as seen in Figure 2.15.

To prevent this effect, signals delayed inside a photonic crystal must have limited bandwidth to prevent dispersion. When the bandwidth is narrow enough that the entire band has the same propagation velocity. In this small range of frequencies, the dispersion diagram will appear to have no curvature.

Useful optical signals generally have wide bandwidths that would typically experience dispersion [35]. Bandwidth compression is necessary, therefore, to be able to use photonic crystals for waveguiding. Such an effect can be realized using time dynamic waveguides.

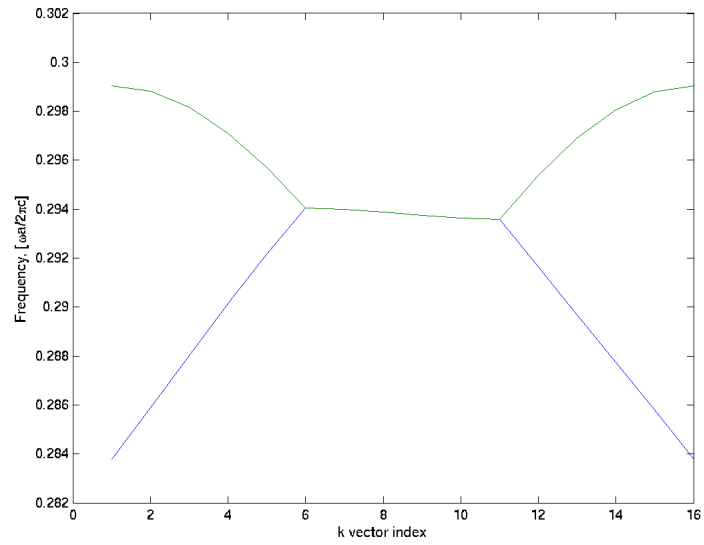


Figure 2.14: Propagating Frequencies of a CROW

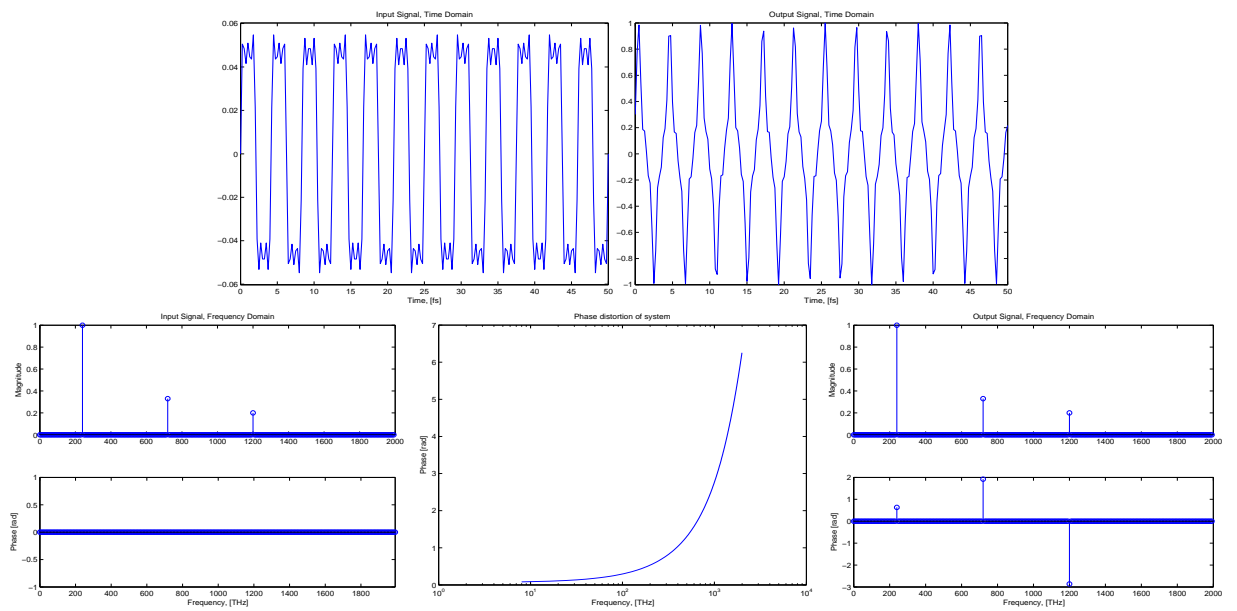


Figure 2.15: Dispersion Due to Nonlinear Phase: The effect of a dispersive system on the square wave is to shift the phase of the frequencies that make it up. This can have drastic effects, as seen in the upper-right figure.

2.5 Time Dynamic Waveguides

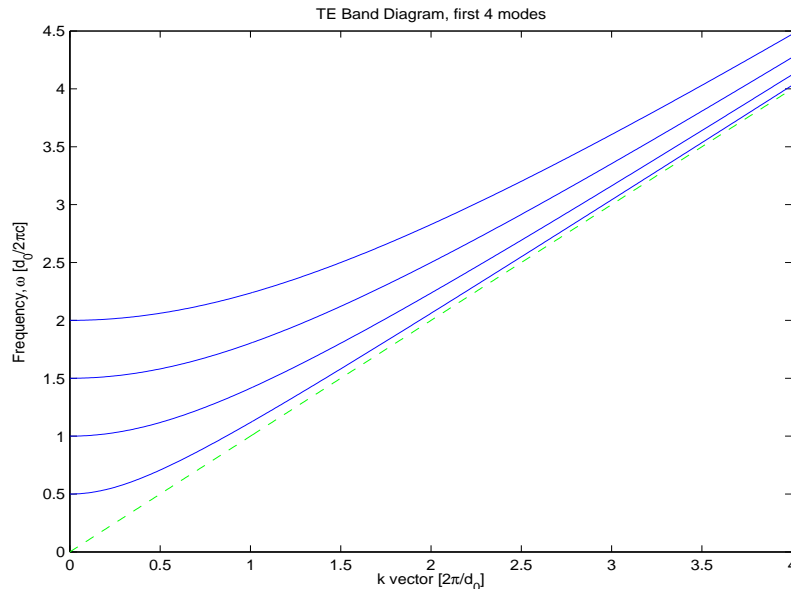


Figure 2.16: Modes of a Parallel Plate Waveguide

Analysis of waveguides with time dynamic characteristics uncovers their interesting properties. For simplicity, the case of the parallel plate waveguide is considered, where the distance between the plates varies linearly with time within a fixed interval, and is fixed outside that interval. It is known that for the parallel plate waveguide, the TM modes have the following properties: $k_c = \frac{n\pi}{d}$, $\omega_c = \frac{k_c}{\sqrt{\mu\epsilon}}$, $v_p = \frac{\omega}{\beta}$, and $\beta = k_z = \sqrt{k^2 - k_c^2}$ where k_c is the cutoff wavenumber, d the distance between the plates of the waveguide, n is the mode number, and v_p is the propagation velocity. The wave impedance is $Z_{TM} = \frac{\beta}{\omega\epsilon} = \frac{\beta\eta}{k} = \frac{1}{v_p\epsilon}$ [20]. Note that the propagation velocity can also be expressed as $v_p = \frac{\omega}{\sqrt{k^2 - (n\pi/d)^2}}$. The TE modes have the same expressions for these values except the wave impedance which is $Z_{TE} = \frac{k\eta}{\beta} = \frac{\omega\mu}{\beta}$. If one plots ω versus k_z one has the familiar dispersion diagram corresponding to the equation $\beta = k_z = \sqrt{(\omega c)^2 - (n\pi/d)^2}$ as seen in Figure 2.16.

Note that each curve (other than the TEM mode) is dependent on the waveguide distance d . If this distance were to change slowly, as to allow an adiabatic transition, the energy

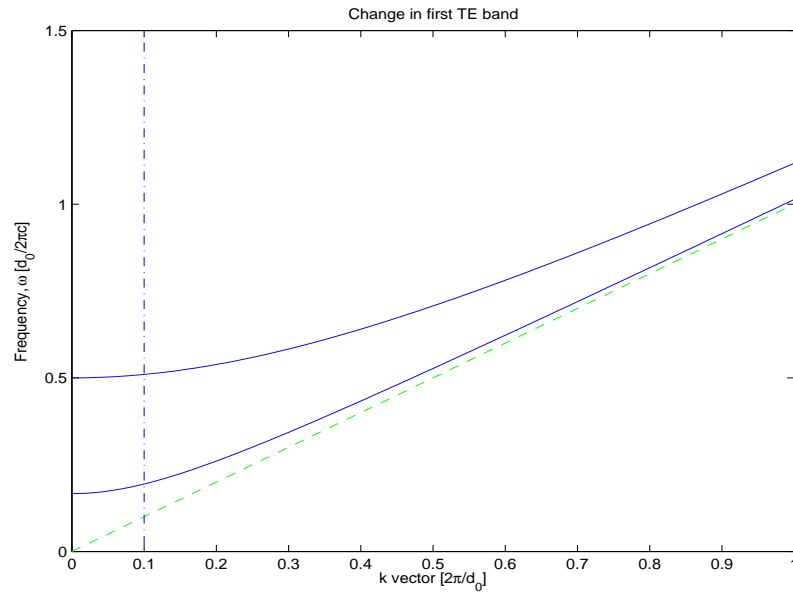


Figure 2.17: Effect on First Mode Due to Time Varying Waveguide

will remain in the mode rather than disperse among the modes as one would expect to occur for a fast transition. Since the plates are moving exclusively in the y direction, the z component of the momentum of the wave cannot be effected by this motion. As a result, k_z does not change during the transition while the curve drops down, so the frequency drops in compensation as seen in Figure 2.17.

As the plates spread apart, one notices that the slope of the band near this k_z point increases with increasing d . This means the group velocity decreases with decreasing d . Thus the propagation can be arbitrarily slowed in such a waveguide.

As the plates are returned to the original positions, slowly to maintain adiabaticity, the band diagram will return to the initial configuration, and the field will return to the original state, with the exception of having added phase due to the time spent in the stored state. In this way, a time varying waveguide exhibits state storage. One also may note that if the field contained a band of frequencies, this band shrinks as d is decreased. Thus the time dynamic waveguide also bandwidth compresses the signal as it is being stored.

The time dynamic waveguide effects described above can be achieved in other ways,

most notably by index changes. In photonic crystals, the changes to the band diagrams can be more exotic and can lead to a complete stoppage of light or even time reversal of light [35].

2.6 Yanik and Fan Structure

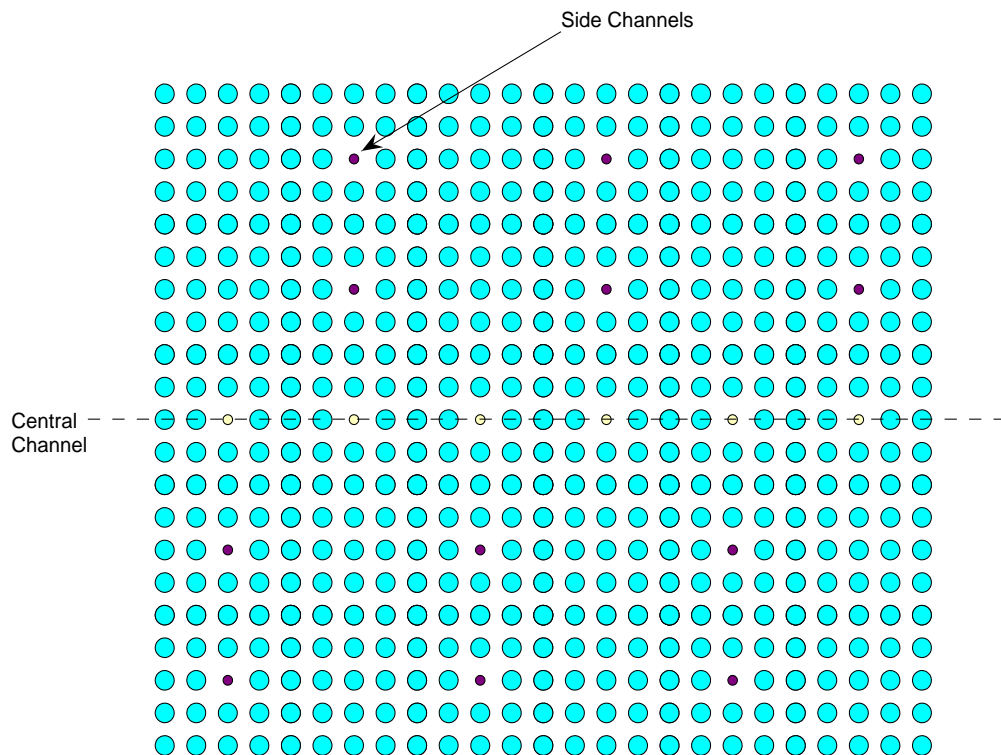


Figure 2.18: Yanik and Fan structure

Yanik and Fan proposed a 2D CROW structure in which an optical signal can be stored for an arbitrarily long time with arbitrarily low dispersion [35]. To realize these effects, the bandwidth of the signal is compressed through the use of a dynamic refractive index on the lattice defects which can be found along the central channel and in the side channels as shown in Figure 2.18. In the figure, the defects can be found along the highlighted areas. The system functions in the following way: first, the signal enters the device and the mode

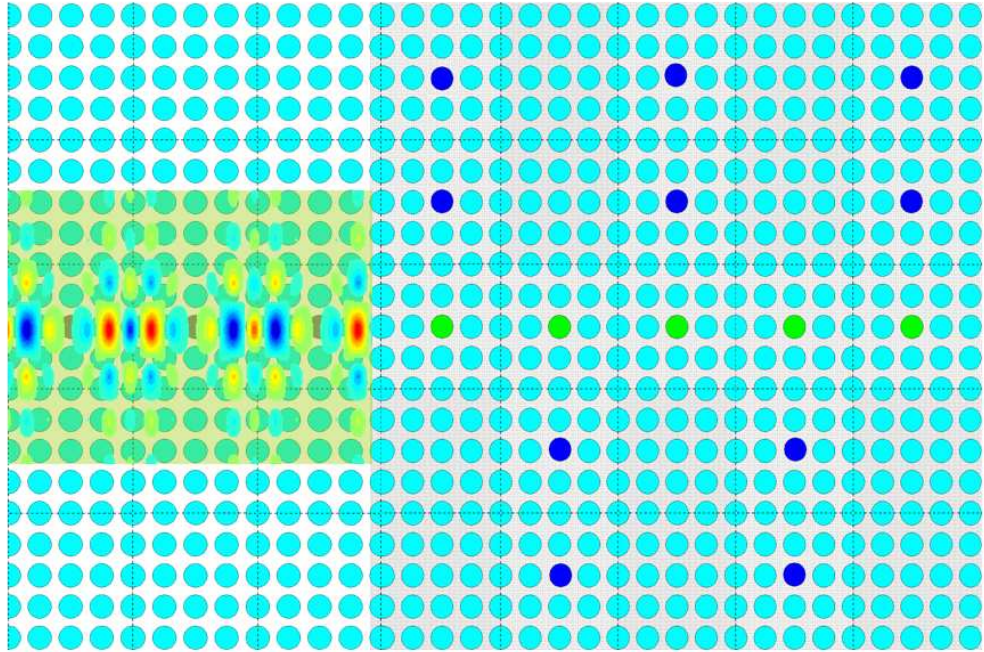


Figure 2.19: Propagating Mode in a CROW: Top-down view

propagates mostly down the central channel. Next, the index is slowly tuned changing the mode that propagates in that band from one that propagates mostly in the central channel to one that propagates along the side channels. This process bends the band to a more horizontal state, so that the bandwidth is compressed. The tuning is done slowly enough that the transition from modes in the central channel to the modes in the side channels is adiabatic. The mode transitions to its counterpart in the new system with negligible losses. When the system is in the state for which the energy stays mostly in the side channels, the mode propagates very slowly. Theoretically the rate at which the mode propagates in this state can be made arbitrarily small by lengthening the side channels [35]. The original mode can be restored by slowly reversing the index changes.

In reference [35] Yanik and Fan illustrate their procedure with two structures, one is

a simple structure with single resonator side chains, relatively high coupling coefficients, and unrealistically large index changes. The second is a more complex structure, with double resonator side chains, lower coupling coefficients, and a realistic index change which is depicted in Figure 2.18.

There are multiple benefits of this system. First, the bandwidth compression negates the effects of phase dispersion that would normally exist. Dispersion is reduced by compressing the bandwidth down to the point that the dispersion relationship is linear for the frequencies in the band. Second, the tunability allows the system to hold the signal for a somewhat arbitrary length of time. Because of this, one could use this structure as an optical flip-flop in the following way: while the control pulse is set to the “pass-through” state, a signal is accepted into the central channel. The control pulse is then switched to the “hold” state, and the signal can be held until it is synchronous with other signals in the overall system, as is done with electronic flip-flops in conventional digital circuits.

Though it would seem that this bandwidth compression scheme has immense benefits, one potential risk stands out, this being possible loss of the stored state due to thermal broadening. One can think of thermal broadening as Doppler shifts in the frequency of the stored light caused by collisions with the vibrating lattice. Since the thermal broadening is occurring while in the bandwidth compressed state, the effect is enhanced when the bandwidth is restored.

2.7 Quantum Mechanics in Dielectric Media

To understand the interaction of the thermal field with the state stored in Yanik and Fan’s structure, one must approach the problem from the perspective of quantum mechanics. In particular, the aspects of quantum theory concerning density of states and spontaneous emission are crucial to gaining insight into this problem.

It is often noted that thermal emission is a special case of spontaneous emission in which the electronic states of atoms are in thermal equilibrium with the surrounding environment [5, 8, 22]. Thus the methods of analysis for spontaneous emission apply to thermal emission. It is well known that the rate of spontaneous emission is proportional to the

density of states by Fermi's Golden Rule (Equation 2.10) for the weak coupling regime,

$$w_k = \frac{2\pi\rho(\omega_k)}{\hbar} |\langle i | H_k | f \rangle|^2 \quad (2.10)$$

where $|i\rangle$ is the initial state, $|f\rangle$ is the final state, H_k is the Hamiltonian corresponding to the mode with wavenumber k , ω_k is the corresponding frequency, and ρ is the density of states, and w_k has units of one over time [5, 8, 27]. Since the Hamiltonian has units of energy, and the density of states has units of states per unit energy, the resulting value has units of states per unit time. This rate determines the spectrum of thermal emission as per equation 2.11 [5, 8]

$$p(\omega) = \frac{1}{4} c \rho(\omega_k) \frac{\hbar\omega}{e^{k_B T} - 1} \quad (2.11)$$

where ρ is the density of states with units of $[Energy^{-1} \cdot (Volume^{-1})]$, c is the speed of light in a vacuum, \hbar is the reduced Planck's constant, and k_B is Boltzmann's constant. More specifically, spontaneous emission is proportional to the local radiative density of states as given by equation 2.12 [27]. This differs from the local density of states by a factor of ε^{-1} [27]. Sprik et al. show that the classical calculation is valid for calculating density of states in the quantum mechanical regime [27].

$$N_{rad}(\mathbf{r}, \omega) = 2\omega \sqrt{\frac{1}{\varepsilon(\mathbf{r})}} \langle \mathbf{r} | \delta(\omega^2 - (-\sqrt{\frac{1}{\varepsilon(\mathbf{r})}} \nabla^2 \sqrt{\frac{1}{\varepsilon(\mathbf{r})}})) | \mathbf{r} \rangle \quad (2.12)$$

Cornelius and Dowling set forth a computational methodology as follows: the transmission and reflection coefficients are computed and these are subtracted from one to determine the absorption. As the emission and absorption must be equal as per Kirchoff's second law, this remaining amount is also the emission [5, 8].

Although the work of Cornelius and Dowling is based on 1D structures, they describe how the method can be expanded to higher dimensional systems [5]. In reference [8], Florescu et al. expand the model to the three dimensional case of an inverted opal photonic crystal.

In lossless materials, the only interaction of the thermal states with the material is via reflection at the material surface. The radiation spectrum from the material is modified by the transmission coefficient of the material. If the index of refraction is a function of frequency, the blackbody radiation curve will be multiplied by the transmission curve.

These emission spectra, reduced because the material is not index matched to the vacuum, are known as “greybody” radiation spectra.

In order for the electromagnetic states of the photonic crystal to interact with the thermal states, at least one material in the system must be at least partially absorptive [8]. Unless the material has some absorption, coupling between the thermal states of the system and the electromagnetic states will not occur. This is intuitive as absorption is the conversion of the electromagnetic states into thermal states. This absorption means that $\epsilon(\mathbf{r})$ or $\mu(\mathbf{r})$ must have a non-zero imaginary part. One difference to note between the case of absorptive material to that of lossless material is that the “penetrating” (evanescent) wave in lossy material is absorbed while, in the lossless material, the energy is present, but cannot be absorbed. This absorption is inversely proportional to the Bloch wave number. The result is that even in the band gap there is absorption into the layers for absorptive materials that coincide with the standing wave of the evanescent field [8].

The thermal radiation spectrum of the photonic crystals described in reference [5] and [8] have the properties that thermal radiation can be entirely suppressed in a complete band gap, and even reasonably reduced in a partial band gap. Meanwhile, outside the band gap the emission of the material oscillates from the level expected for the absorptive dielectric to the blackbody radiation level, where the reflection coefficient at the material interface normally leads to a spectrum lower than that of a blackbody at the same temperature for absorptive “greybody” dielectric materials [5].

Though thermal effects have been studied in bulk photonic crystal materials, little study has been done on these effects in the coupled resonator optical waveguide (CROW) structure, in which coupling between resonator defects allows a propagating mode in what was the band-gap of the bulk material [37]. One such system is that proposed by Yanik and Fan in which an optical signal can be stored for an arbitrarily long time with arbitrarily low dispersion through the use of a dynamic refractive index on the lattice defects [36].

Chapter 3

Electromagnetic Analysis of the Yanik and Fan Structure

In order to perform the quantum analysis, a numerical analysis of the classical electromagnetic field was first performed to acquire the density of states for the systems to be analyzed as well as the band diagrams for these systems.

The systems that were chosen for analysis were a simple structure with single side channel resonators which requires an unrealistic index change of 10 percent to operate, as well as a more realizable version with side channels that are made up of two resonators and only requires an index change of 0.01 percent, both mentioned in [36]. The former will be referred to as the “simple Yanik and Fan structure” throughout this paper while the latter will be referred to as the “realistic Yanik and Fan structure”.

The modes and dispersion diagrams were calculated in MPB and the data were analyzed in MATLAB. In general, it was found that for both the simple Yanik and Fan structure and the realistic version of structure, the fast propagating mode traveled down the waveguide with most of its energy in the central channel, while the slow mode in both structures had its energy in the side channels as it propagated down the waveguide. The shifting of the bands was observed including bandwidth compression and propagation velocity changes.

The density of states was generated numerically by calculating the frequencies associated with an evenly spaced grid of points in reciprocal k space using MPB. The points were

spread over a single irreducible Brillouin zone. The density of the frequencies associated with evenly spaced points in k space approaches the density of states in the limit. This produces a numerical result for the density of states that can be used in determining the rate at which the coherent state within the CROW structure interacts with the thermal field. To scale these discrete density of states to be in the same units as the continuous density of states, the result must be normalized by multiplying by the spacing between the points in each dimension.

3.1 Modes and Band Diagrams of the Simple Yanik and Fan Structure

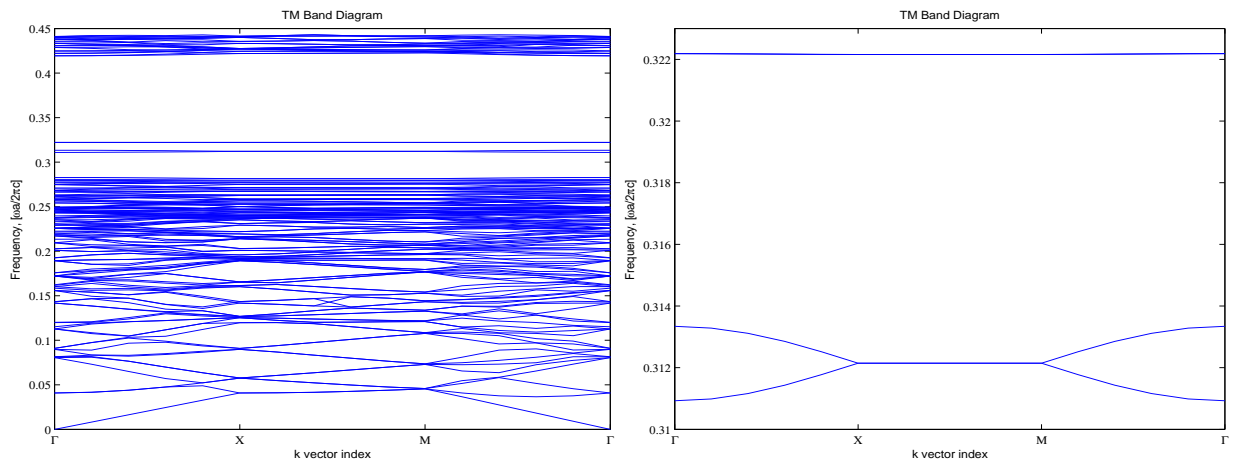


Figure 3.1: Dispersion Bands for Simple Yanik and Fan Structure: The figure on the right shows a zoomed in version of the guided bands

The simple Yanik and Fan structure has two pairs of bands in the band gap of the original lattice, as seen in Figure 3.1. If the index of the channel and the index of the side channels are shifted away from a central value, the upper band and lower band will compress and expand from a balanced width. The change in index for this simple case was 8% of the nominal value of 3.46. As one can see from Figure 3.2, time reversal can be observed for the lowest band in the band gap as the band changes from positive to negative

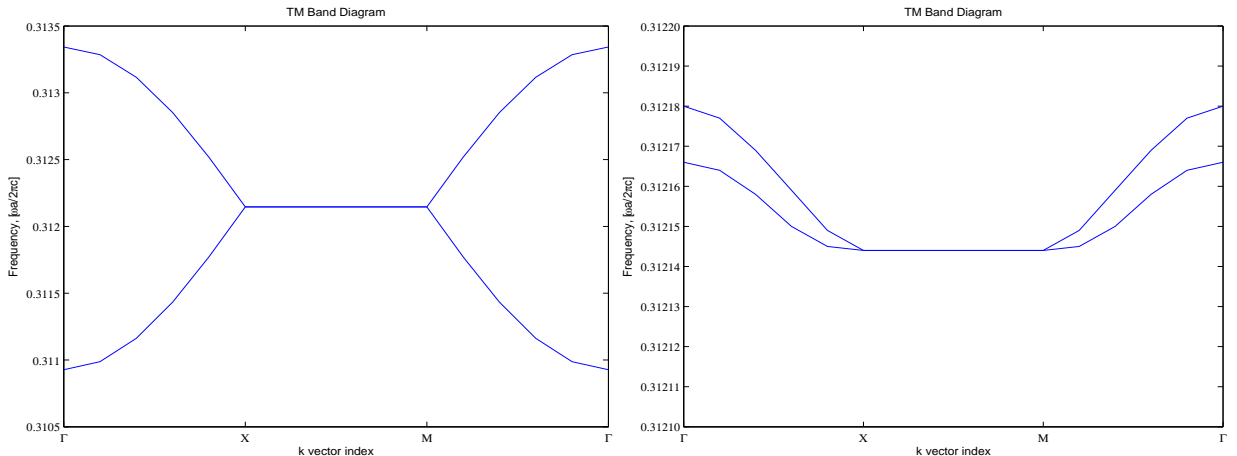


Figure 3.2: Comparison of Bands for Simple Yanik and Fan Structure in the Propagating State (Left) and Storage State (Right)

slope. As a result, arbitrary bandwidth compression can be achieved for this structure, if a smaller index change is used in the lowest band, or if the second lowest band is used. As one can also see from Figure 3.2, the bandwidth that the simple Yanik and Fan structure accepts is $1 \cdot 10^{-3}$ in normalized frequency. Because the band occurs around .312, the ratio of the center frequency to the bandwidth can also be expressed as a Q of 3000. For a 200 THz optical signal, the bandwidth corresponding to the “pass-through” state is 67 GHz. The Q of the stored state would theoretically be infinite according to this model, however, it will actually be limited by losses in the dielectric and scattering. The following sections will show that the input bandwidth of the realistic structure is not nearly as wide as the bandwidth is for this simple structure.

As with other high Q resonators, it is difficult to couple into the storage state. One benefit of this system, however, is that the signal will be coupled into the lower Q “open” state and once coupled into that state, it becomes easy to couple into the higher Q storage state when the bandwidth is adiabatically compressed.

In the simple Yanik and Fan structure, the energy of the mode is concentrated along the central channel when the system is in the “pass-through” state as seen in Figure 3.3. In contrast, Figure 3.4 demonstrates that the storage mode of the simple Yanik and Fan

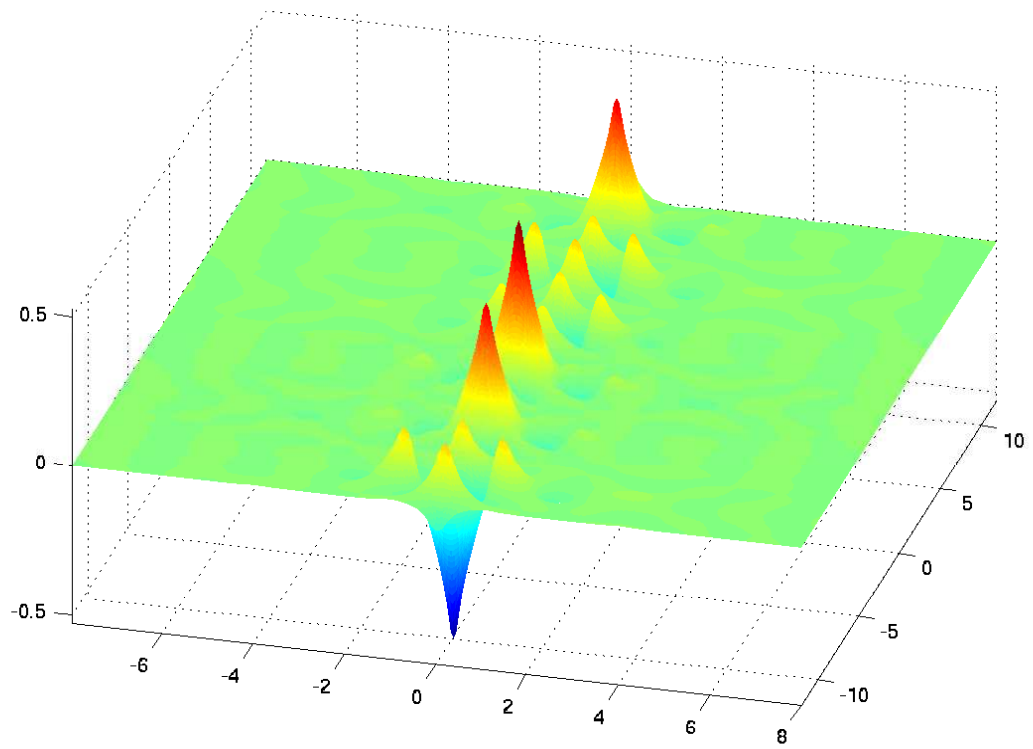


Figure 3.3: The Propagating Mode of the Simple Yanik and Fan Structure (Normalized Electric Field Amplitude, x and y Displacement Normalized to the Lattice Constant)

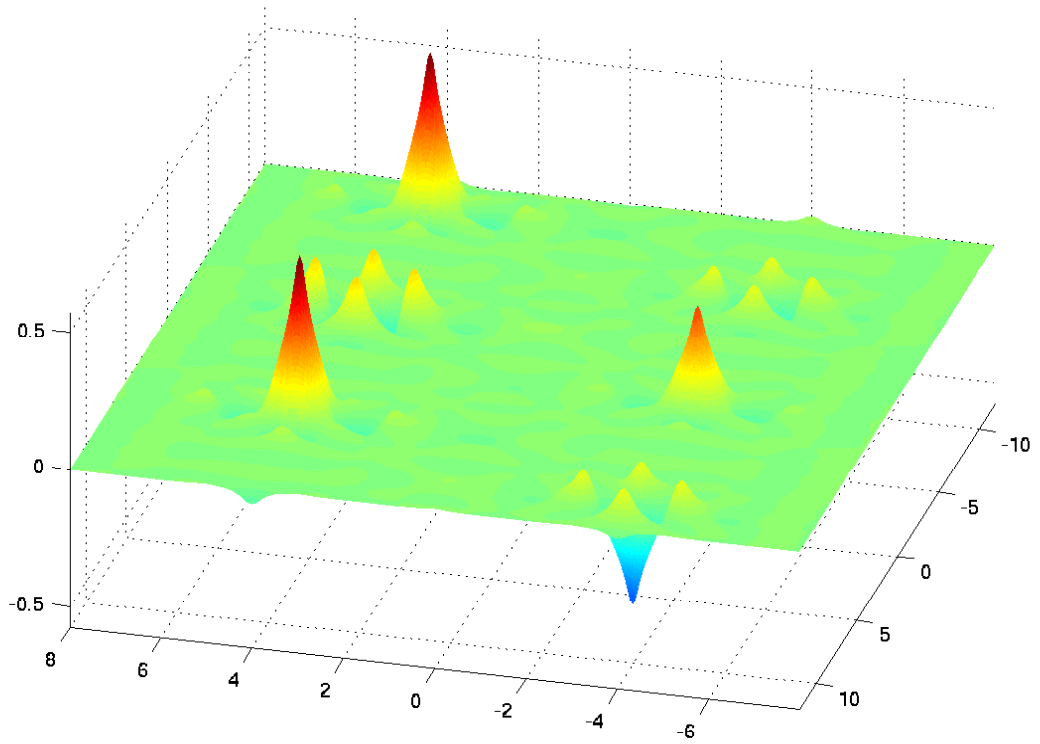


Figure 3.4: The Stored Mode of the Simple Yanik and Fan Structure (Normalized Electric Field Amplitude, x and y Displacement Normalized to the Lattice Constant)

structure has its energy concentrated along the side channels. In both cases, the mode shape is a concatenation of the single resonator mode shape from the previous chapter over each of the active resonators.

While the input bandwidth and compression are adequate for this design, realizing a change of 8% in refractive index is far from trivial. Electro-optic methods provide optics changes of 0.01%, while methods such as applied pressure and magnetic tuning of index of refraction yields changes of 0.5% [23, 34]. Because of this, analysis on a method that requires much less index change is investigated.

3.2 Modes and Band Diagrams of the Realistic Yanik and Fan Structure

As in the case of the simple Yanik and Fan structure with 8% index change, the storage state of the realistic Yanik and Fan structure has most of the energy stored in the side channels. For the propagating state, Yanik and Fan state that the mode energy should be concentrated along the central channel [35].

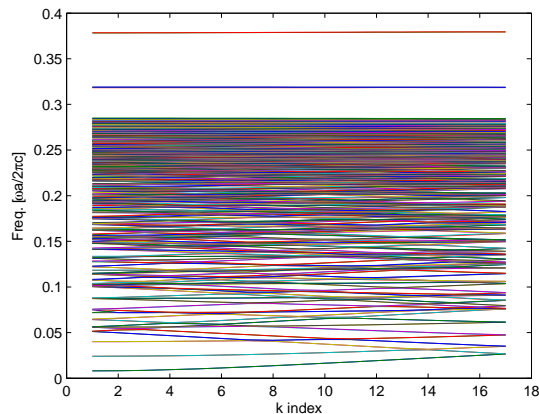


Figure 3.5: Bands for the Realistic Yanik and Fan Structure in the Storage State

Figure 3.5 shows the bands and the band gap for the realistic Yanik and Fan Structure.

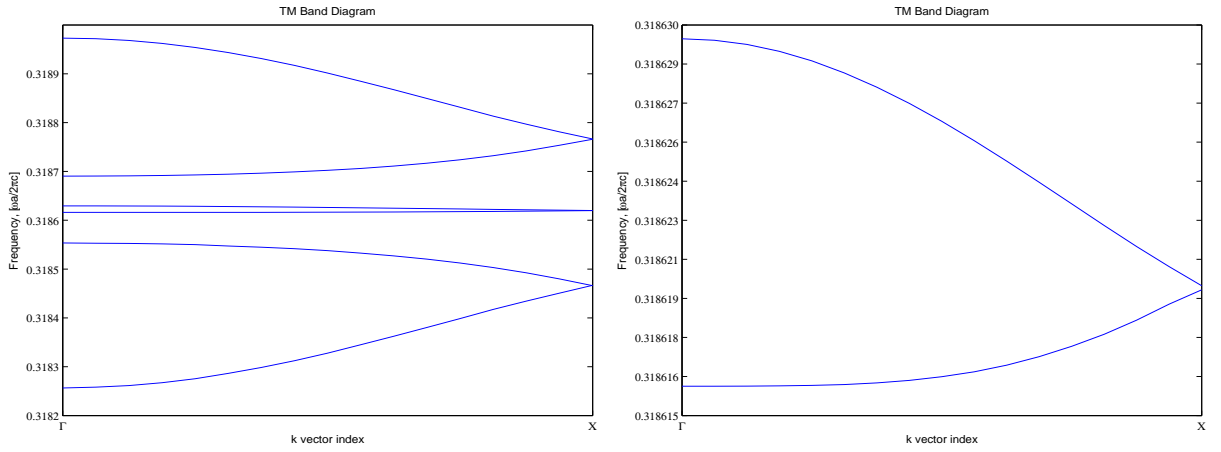


Figure 3.6: Bands in the Band Gap of the Realistic Yanik and Fan Structure in the Propagating State

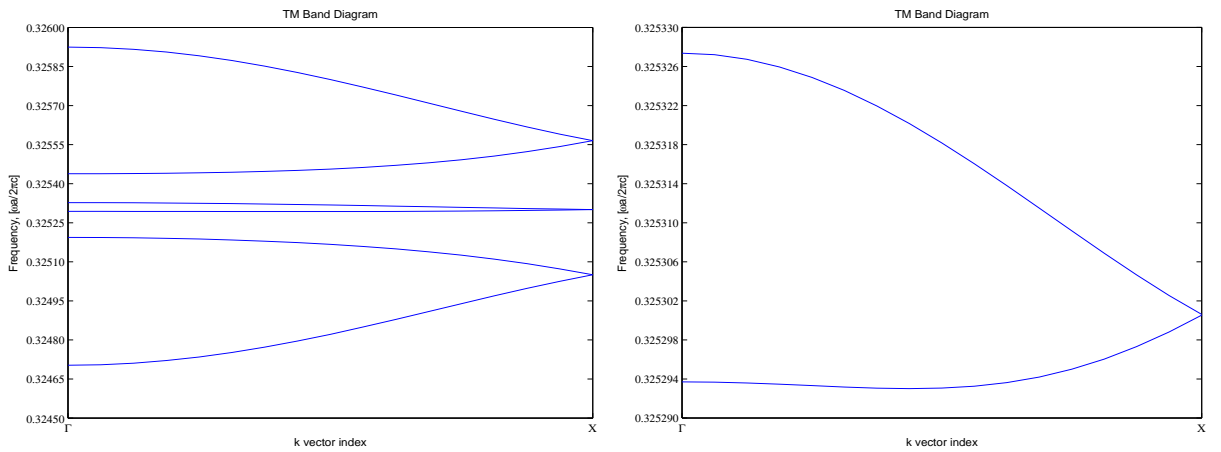


Figure 3.7: Bands for the Realistic Yanik and Fan Structure in the Storage State

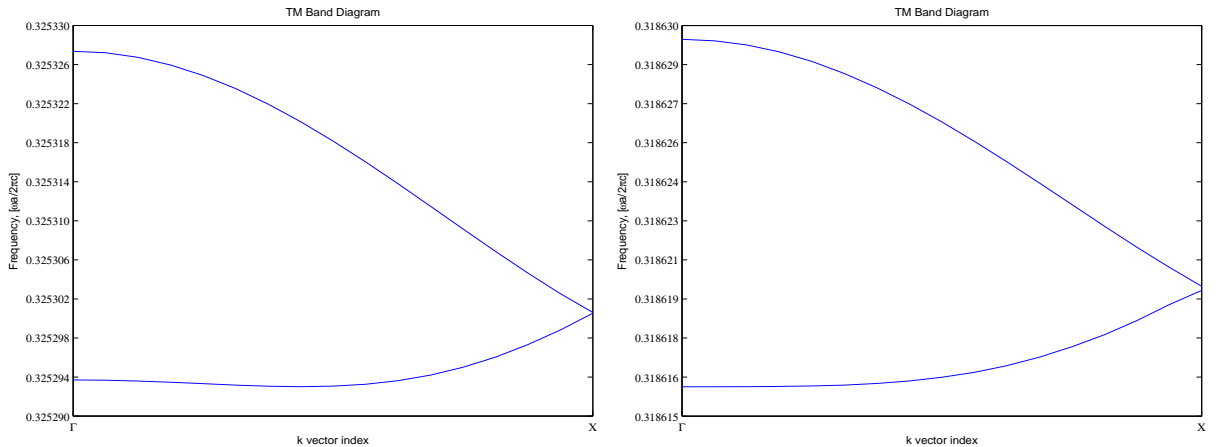


Figure 3.8: Comparison of Bands in the Band Gap of the Realistic Yanik and Fan Structure in the Storage State (Left) and Propagating State (Right)

The band gap of this structure can be found from 0.28 to 0.37 in normalized frequency, interrupted by the guided bands. There are six guided bands for the realistic Yanik and Fan structure as seen in Figures 3.6 and 3.7. In terms of normalized frequency, the realistic Yanik and Fan structure accepts a bandwidth of less than $3 \cdot 10^{-6}$ in the “open” state, which, along with its center frequency of 0.3186 can be expressed as a Q of 110000. The corresponding bands can be seen in Figure 3.6. In the storage state, while the Q of the overall band decreases to 50000 with a center frequency of 0.3253, a portion of the band with a group velocity of zero, where the band flattens to zero slope as seen in Figure 3.8. In order to use this region, the input signal must have a bandwidth of less than $1 \cdot 10^{-6}$. This would map to a bandwidth of only 670 MHz, which is narrower than even the most state of the art optical system by more than an order of magnitude.

It is also important to note that there is a section of the band lower band in Figure 3.8 with a normalized k vector of approximately 0.25 in the k_x direction that has a propagation velocity of $1 \cdot 10^{-7}c$ in the “pass through” state, and has a propagation velocity of zero in the storage state.

3.3 Density of States for the Simple Yanik and Fan Structure

The density of states was generated numerically using MPB and MATLAB. The result from the numerical calculation will be a number of points in k space associated with each range of frequencies. To convert this to an actual density of states, the result must be normalized for the quantization in k space and frequency. Since the structure had previously been normalized in k space, renormalization entails simply dividing by the number of points in a unit cell. Because the material is uniform in the third dimension, by selecting a single layer of points in k space the result is effectively normalized to a lattice constant in this dimension by multiplying by the same factor. The DOS will also have to be normalized in the frequency domain based on the resolution chosen for the histogram.

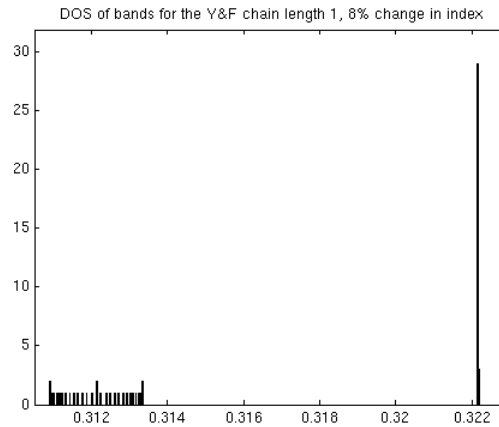


Figure 3.9: Density of States in the Band Gap of the Simple Yanik and Fan Structure, Histogram Bin Size = $5.9375 \cdot 10^{-7}$

The density of states was calculated for both the simple Yanik and Fan Structure where the index of the variable rods changes by 8% and the more realistic case where the index changes by a factor of only 10^{-4} . The result for this case set in both the storage and pass through states can be seen in Figures 3.10, and 3.11. The density of states increased as the bandwidth compressed, such that the total number of states remained constant for both cases.

One can see from Figure 3.9, the density of states increases as the bandwidth is compressed, such that every state in the uncompressed band corresponds to a state in the compressed band. Since the DOS is higher, the probability of transition between these states, via interaction with the lattice, increases.

3.4 DOS in Realistic Yanik and Fan Structure

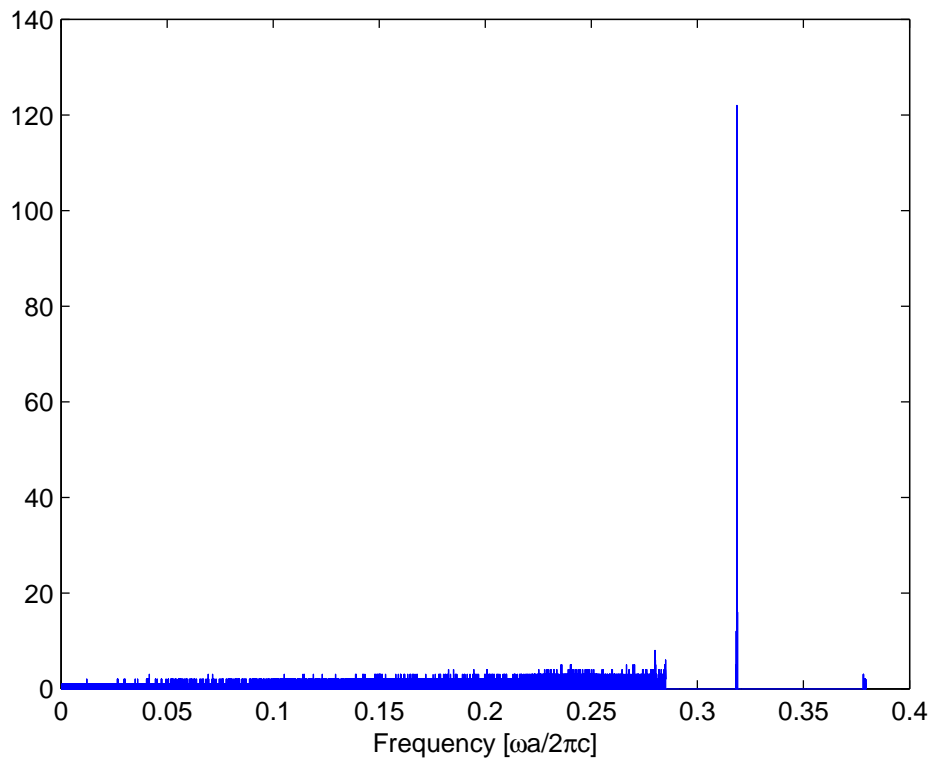


Figure 3.10: Density of States in the Realistic Yanik and Fan Structure, Histogram Bin Size = $5.9375 \cdot 10^{-7}$

The density of states was generated for the both realistic Yanik and Fan states using 153 evenly spaced k points in the irreducible Brillouin zone, which corresponds to a linear spacing of $\frac{1}{32}$ in normalized k space. The normalized frequency range of .38 was quantized into 640000 bins for the histogram, thus each bin had a bandwidth of $5.9375 \cdot 10^{-7}$ in

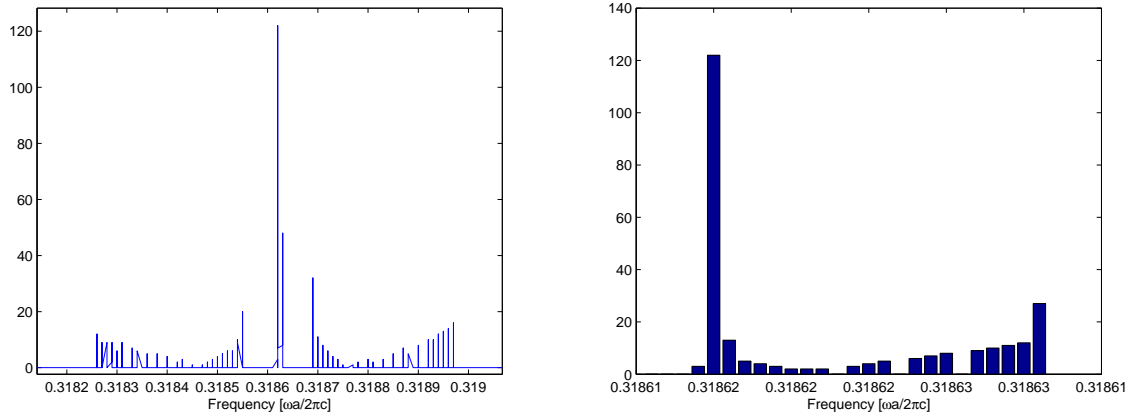


Figure 3.11: Density of States for the Realistic Yanik and Fan Structure in the Storage State, Histogram Bin Size = $5.9375 \cdot 10^{-7}$

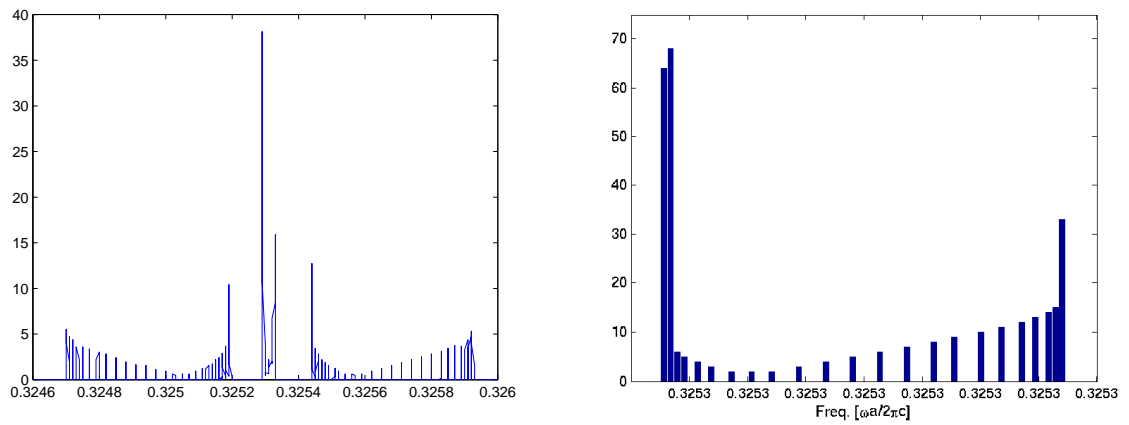


Figure 3.12: Density of States for the Realistic Yanik and Fan Structure in the "Pass Through" State, Histogram Bin Size = $5.9375 \cdot 10^{-7}$

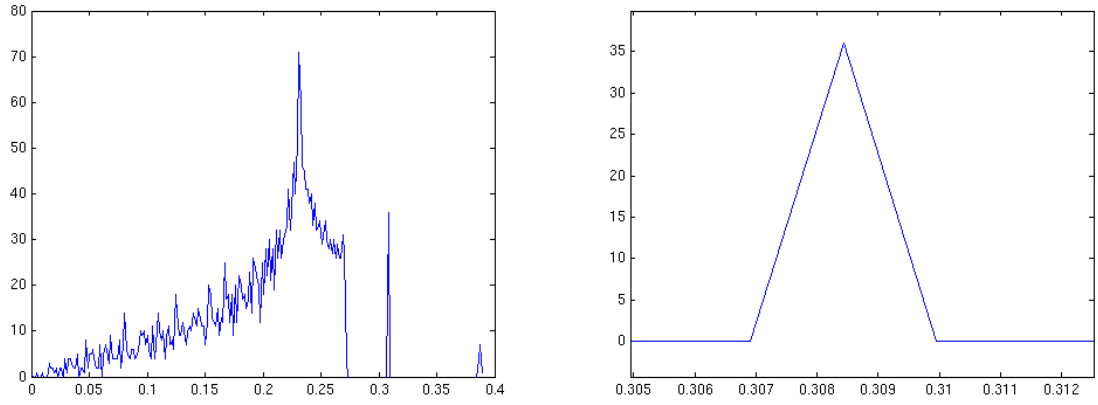


Figure 3.13: Density of States for the Realistic Yanik and Fan Structure in the Storage State, Histogram Bin Size = $5.9375 \cdot 10^{-7}$

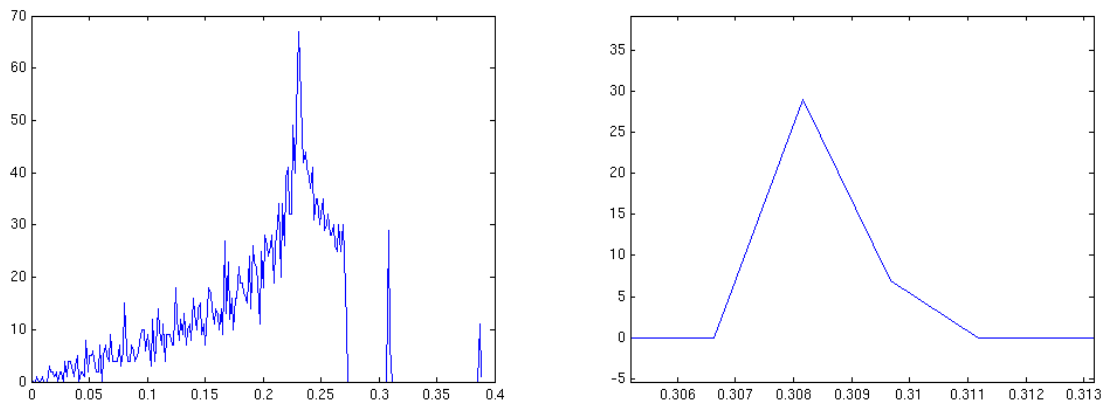


Figure 3.14: Density of States for the Realistic Yanik and Fan Structure in the "Pass Through" State, Histogram Bin Size = $5.9375 \cdot 10^{-7}$

normalized frequency.

Since the density of states increases with bandwidth compression; as one would expect, the transition probability goes up for the realistic structure as well. The density of states for the realistic Yanik and Fan structure can be seen in Figure 3.10. If one looks closely at what appears to be a single peak in the band gap as in Figure 3.11 one sees that there are actually 3 bands, and the central band is the one that exhibits bandwidth compression

3.5 Outcome of Electromagnetic Analysis

In the Yanik and Fan storage structure, the bandwidth compression, and hence the phase distortion, is a function of the coupling coefficient between the resonators and the index change of the defects [35]. Because the index change of the EO tunable index materials is maximized at high index, the index of all the rods is chosen at the maximum index [22]. For EO tunable devices, this maximum index of refraction is typically 3.5 for gallium arsenide [22]. Another thing to note is that the bandwidth of these modes is rather narrow. The ratio of bandwidth of the center frequency for the example shown above is less than 1%. This ratio would shrink down to around 0.01% if one were to change the system to one which is able to use EO tunable materials to perform the index changes. To put some real values on the system, the bandwidth of the 1260 nm - 1360 nm O-Band, (one of the most commonly used optical transmission spectra) is 17.5 THz, or 7.6% of its center frequency 230 THz. The simple Yanik and Fan structure would have an input bandwidth of 67 GHz, which would be considered narrow for optical systems, while the realistic Yanik and Fan structure has a bandwidth that is over an order of magnitude lower. 67 GHz is, for example, on the order of a single band of state of the art 3 Tbps OFDM optical transmission systems.

Chapter 4

Application of Quantum Analysis to CROWs

This chapter will first detail the more general case of quantum mechanics in crystalline solids. The methods can then be expanded to lattices of such media. This will be followed by a discussion of adiabatic transitions between states, using the Yanik and Fan structure as an example. Finally, conclusions will be drawn from what is found.

4.1 Quantum in Crystalline Solids

The classical electromagnetic fields are closely related to quantum mechanics. In fact, the electric field is sometimes treated as the wavefunction of the photon [25]. The treatment known as the semi-classical treatment predicts most quantum phenomenon, such as stimulated emission and Rabi oscillation. In the semi-classical approximation, atoms are treated quantum mechanically while the electromagnetic field is treated classically. Semi-classical models of spontaneous emission have been deemed “unsatisfactory” [18]. It arises directly from the zero quantum state of the quantized electromagnetic field having non-zero energy. While the semi-classical approximation does not predict single photon effects, it does predict the expected value of the number of photons in the field. For fields of many photons in magnitude, the continuous predicted magnitude is sufficiently close to the actual quantized

magnitude.

4.1.1 Dipole Approximation

The semi-classical approximation is often further simplified to the dipole approximation. The dipole approximation of the electric field ignores the effects of quadrupole interactions and magnetic interactions. In many cases, this simplification can greatly simplify quantum analysis with negligible loss in accuracy.

Photons with energies below the x-ray region have wavelengths much larger than that of the size of the atomic lattice. The result of this is that the entire atom is approximately exposed to a spatially constant electric field. The magnetic field interaction and quadrupole interaction are also negligible until the wavelength of the photon approaches the size of the atom. As a result, dipole approximation is well suited for the purpose of analysis of quantum interactions with matter at optical frequencies. [12]

4.2 Phonons in Crystalline Solids

The quantized thermal states of a material are described using phonons. Because phonons arise from the harmonic oscillator Hamiltonian with periodic boundary conditions, they are mathematically analogous to the electromagnetic field in a photonic crystal lattice. Analogies include the existence of dispersion relations for propagating mechanical waves within the material and the presence of band gaps within these dispersion relationships. The energy of a phonon is $\hbar\Omega(k)$ where $\Omega(k)$ is the dispersion relation evaluated for a phonon with wavenumber k .

The lowest band of phonon energies is known as the acoustic band. The maximum energy of this band is material dependent but is never higher than $\frac{\hbar v_s}{a_0}$ where \hbar is Planck's constant, v_s is the speed of sound in the material and a_0 is the atomic lattice spacing of the material. So for example, in silicon, which has a v_s of 6400 m/s and an a_0 of 0.357 nm, results in a maximum phonon energy of about 40 meV which will only couple well with photons that have comparable energy, thus electromagnetic energy with frequencies above 10 THz does not couple well to the acoustic band. As a result, interactions with optical

frequencies typically require multi-phonon interactions which are generally less likely to occur than single phonon interactions, since the transition probability decreases as a power law as the number of phonons required for the interaction increases.

In the special case where the material has a lattice made up of more than one type of atom, as is the case in the zincblende gallium arsenide (GaAs), optical energies can interact with single phonons. Such systems have upper phonon energy bands known as optical bands because they interact more easily with optical energy. The bands of phonon energies originate from the asymmetric interaction between the atoms of different masses. Lattice defects are another cause of direct absorption of photons. The phonon bands of gallium arsenide extend from energies starting at zero to a maximum of 36.6 meV, which corresponds to a frequency of 8.85 THz and a wavelength of 33.9 μm [3]. As a result, this direct mode of thermal interaction is very unlikely for near-infrared optical transmission frequencies. Expanding to the case of photonic crystals, the methods similar to those used earlier for treating electromagnetic fields in periodic boundary conditions can be applied. Since the period of most conceivable photonic crystal structures is associated with such a low energy phonon, the phonon bands are not perceivably affected by the limited size of each structure.

As you can see from Figure 4.1, in the band gap the density of states is zero. One may also note that there is an enhancement of the DOS near the band edge. These are common features of photonic band gap materials.

One notes that when there is a defect, though most of the density of states remains unchanged, a density of states is created inside the band gap due to the introduced defect mode as seen in Figure 4.2. This is analogous to how allowed states appear in the band gap of a semiconductor when doped [14].

4.3 Yanik and Fan Structure

The Yanik and Fan structure is made up of strings of resonators. The approach used to analyze the single resonator can then be expanded to the case of CROWs in general and the Yanik and Fan structure in particular.

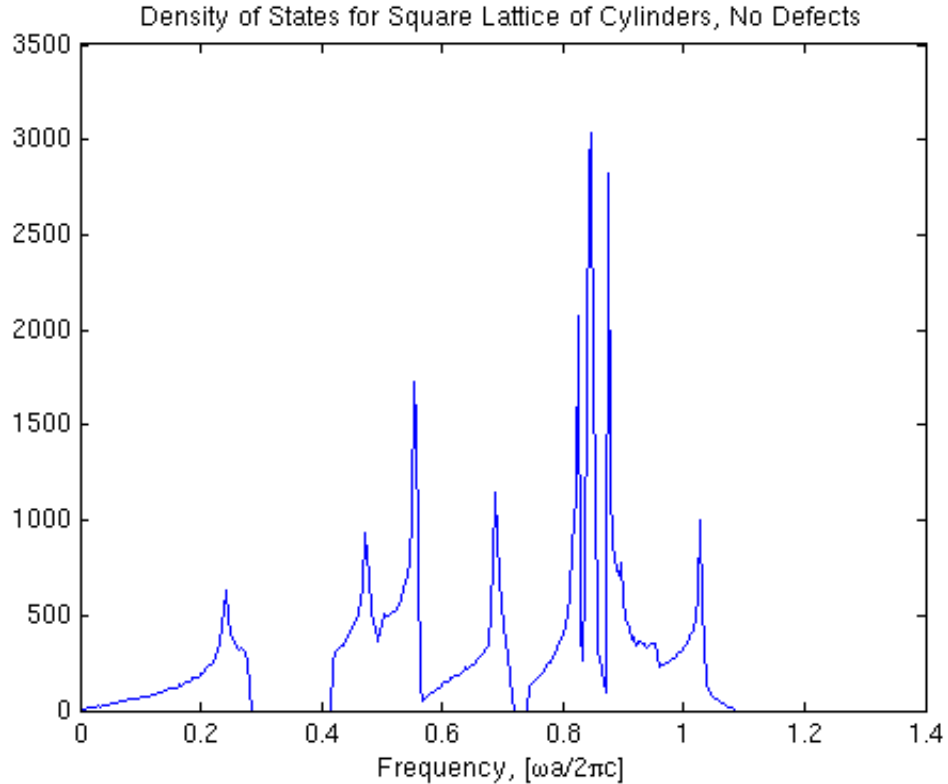


Figure 4.1: DOS of a 2D Square lattice, Histogram Bin Size = $5.9375 \cdot 10^{-6}$ in Normalized Frequency

In storage state, the Yanik and Fan structure is essentially a resonator cavity, albeit a complex resonator made up of a lower hierarchic level of resonators. Resonator cavities are known to preserve the quantum state of the field stored within them. The primary example of this effect is the preservation of the quantum state in a laser cavity. One question which arises in this case is whether the quantum state is preserved during transition between the pass-through state and the storage state.

4.4 Adiabatic Tuning of the Basic Structure

Yanik and Fan point out that in order for the state to be maintained during transitions, these transitions must be adiabatic. In order to have an adiabatic transition, the perturba-

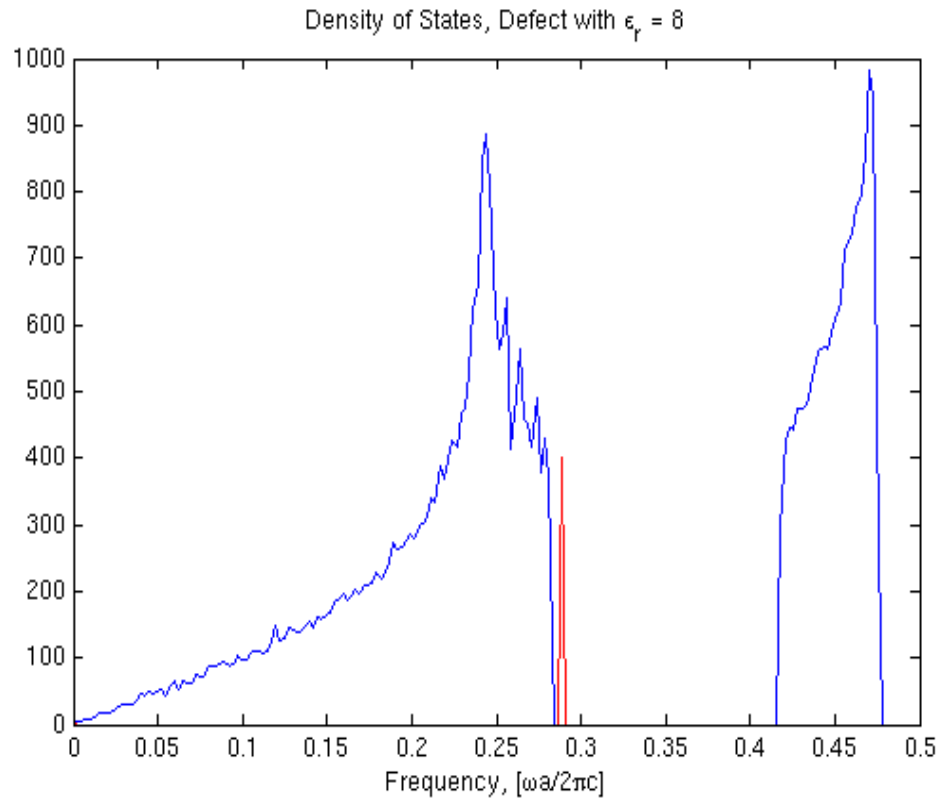


Figure 4.2: DOS of a 2D Square lattice with defect, Histogram Bin Size = $5.9375 \cdot 10^{-6}$ in Normalized Frequency

tion of the system must be much slower than time period associated with the difference of the energy levels present. If one transitions too quickly, the energy of the initial state will be dispersed into the other states, to the limit where if one transitions instantaneously, the coupling to each band will be proportional to the projection of the original mode onto the modes of the final system [4, 12]. In both the realistic and simple structures described by Yanik and Fan, there is inherently at least one nearby band that requires the transition to occur very slowly.

4.5 Conditions for Maintaining Adiabatic Transitions

The time $t_{A \rightarrow B}$ required to maintain an adiabatic transition is that which satisfies the inequality:

$$t_{A \rightarrow B} \gg \left[\frac{E_i - E_j}{\hbar} \right]^{-1} \quad (4.1)$$

for all energy levels E_i and E_j , $E_i \neq E_j$, throughout the transition [12]. The nearest bands can interact most strongly. If one selects non-degenerate portions of the bands from Figures 3.2 and 3.8, the spacing of these nearest bands is $1 \cdot 10^{-5}$ in normalized frequency for the simple Yanik and Fan structure. This band spacing requires the transition time to be much greater than 0.15 nanoseconds for an optical transmission frequency of 200 THz. For the realistic Yanik and Fan structure, the spacing between the bands is $1.3 \cdot 10^{-5}$, which corresponds to the requirement that the transition time be greater than 0.12 nanoseconds. Because of this, transitions in the simulation had a duration of at least one nanosecond.

One may recall from in Figures 3.2 and 3.8 that the dispersion bands of the propagating modes intersected at the X point. Since this point is degenerate, an adiabatic transition could never occur if energy was stored at with this k vector. If the energy of the stored field While this section of dispersion diagram would have represented a useful portion of the simple Yanik and Fan structure's band, the realistic structure does not exhibit bandwidth compression near the X point; rather, the greatest bandwidth compression for the realistic Yanik and Fan structure occurs near midpoint between the Γ and X point.

4.6 Other Quantum Effects

There are other quantum effects to consider, with varying degrees of likelihood that one will encounter them in photonic crystal CROW structures. These include electron hole pair generation and electric quadrupole and magnetic coupling effects. This section will discuss how these effects might arise in photonic crystal structures.

Electron-hole pair production would be the first significant quantum effect that would be encountered as one deviates from the standard optical bands. The band gap for gallium arsenide, for example, is approximately 1.5 eV, which is the energy of a 830 nm photon.

Because of this, gallium arsenide should not be used in the waveguiding of the 850 nm infrared band due to the high absorption at this wavelength. As the photon energy increases through the optical region, the absorption would increase, eventually beyond the level of absorption at the band gap resonance [3].

Although there are far greater problems in using energies above the optical region in lattices, it may be interesting to discuss what effects might occur. In the x-ray region, quadrupole coupling and magnetic coupling will become pronounced because the wavelength approaches the lattice constant of the constituent dielectric crystal [12]. These additional coupling mechanisms cause degeneracy at the associated energies. One should note that a photonic crystal structure for the x-ray region would have its structure at the atomic level. If photonic crystal structures are designed for x-rays the quadrupole and magnetic coupling effects must be considered.

Chapter 5

Thermal Spreading

In a dielectric material, thermal interactions with the electromagnetic field are governed by the atoms contained in the material. If the dielectric is crystalline, these atoms are in a periodic lattice. Thus, for crystalline dielectric materials, the equations for the interaction between a unit cell of the crystalline lattice and the electromagnetic field are valid and periodic boundary conditions can be used.

5.1 Classical Thermal Losses

Thermal losses in the dielectric are generally accounted for in standard waveguides and resonators with a complex ϵ and μ [20]. This leads to a solution for the field that has a term that decays exponentially with time. This attenuation factor is known as α , and is the real part of the solution to the wave equation

$$\omega\sqrt{\mu\epsilon} = \gamma = \alpha + j \cdot k \quad (5.1)$$

for the case of constant μ and ϵ , where γ is the complex propagation constant and α and γ have units of m^{-1} [20]. This is also directly related to the loss tangent, which is the ratio of the imaginary part of ϵ to the real part, assuming no magnetic losses, and conveys the ratio of the absorption to the period of oscillation. The quality factor “Q” can be defined as the reciprocal of the loss tangent [29].

Gallium arsenide is highly absorptive of light with photon energies near its band gap

energy of approximately 1.5 eV, corresponding to a wavelength of 830 nm. The absorption coefficient at this wavelength is on the order of 8000 cm^{-1} [3]. The attenuation factor for intrinsic gallium arsenide improves to less than 0.3 cm^{-1} for wavelengths longer than 1000 nm [26]. The attenuation factor can be used directly to find the quality factor, Q , of the dielectric. Using the equations [20]:

$$\gamma = \frac{j\omega\sqrt{\epsilon_r}}{c} \quad (5.2)$$

$$\gamma = \frac{j\omega\sqrt{\epsilon_r'}\sqrt{1+j\cdot\tan\delta}}{c} \quad (5.3)$$

$$\alpha = \text{Re}(\gamma) \quad (5.4)$$

$$Q_d = \left| \frac{1}{\tan\delta} \right| \approx \left| \frac{\epsilon_r'}{\epsilon_r''} \right| \quad (5.5)$$

where $\epsilon_r' = \text{Re}(\epsilon_r)$ and $\epsilon_r'' = \text{Im}(\epsilon_r)$, one can derive an expression for Q in the case that $\tan\delta \ll 1$:

$$\gamma \approx \frac{j\omega\sqrt{\epsilon_r}}{c} - \frac{\omega\sqrt{\epsilon_r}\tan\delta}{2c} \quad (5.6)$$

$$\alpha \approx \frac{\omega\sqrt{\epsilon_r}\tan\delta}{2c} \quad (5.7)$$

$$Q \approx Q_d \approx \frac{\omega\sqrt{\epsilon_r}}{2\alpha c} \quad (5.8)$$

This factor would result in a Q of 25000 to 100000, which is somewhat higher than one expects from high quality dielectrics. The storage lifetime, τ , of a signal can be expressed as [29]:

$$\tau = \frac{Q}{\omega} \quad (5.9)$$

The resulting storage lifetime is on the order of one nanosecond for a 200 THz signal for the system detailed above.

For the infrared frequencies used in optical transmission, the free carrier absorption is the main loss effect [3]. The valance and conduction bands of gallium arsenide span several electron volts [3]. As a result, a mobile electron or hole can absorb a photon and change energy levels within the respective band. One should note that these losses are highly dependent on doping, and heavily doped semiconductors have higher absorption, and this absorption is roughly proportional to carrier concentration [26].

While the modes are more complex for photonic crystals, the solution remains the original mode for the lossless dielectric case, which experiences an exponential decay with time. For the photonic crystal structures studied, the field in the waveguide bands has most of its energy in the higher index dielectric component of the photonic crystal structure. As a result, the attenuation of the field in the photonic crystal will be on the order of this dielectric material.

The first correction for this model is generally to account for nonlinear effects by allowing for frequency dependent ϵ and μ with a frequency dependent attenuation factor. In the case of the narrow bands for the photonic crystal in the storage state, this effect will be negligible. Using this approximation, the entire stored band will experience one effective dielectric constant, with a constant attenuation factor.

The attenuation factor directly widens the bands of the dispersion diagram so that each becomes a band instead of an infinitesimally thin line. The bandwidth widens according to the equation [29]

$$BW = \frac{\omega_c}{Q} \quad (5.10)$$

where BW is the bandwidth in radians per second and ω_c is the frequency stored. The bandwidth of the band of interest in the Yanik and Fan structures are mapped to a optical transmission frequency 200 THz and a quality factor of 100000 as outlined above, the result is that the band is widened to 2 GHz. Because the widening is caused by multiple independent interactions, the result is that the band is Gaussian in frequency. When the bandwidth of the signal is compressed by tuning the structure, the widening of this band does not change because the processes that cause the losses are unaffected.

When the signal attenuates in the classical model, how the energy is distributed is not described, only that it is dissipated in the material. There must be a description of the interaction of the stored state with the thermal field in order to explain how the electromagnetic field evolves due to this interaction. To do this we must return to quantum mechanics.

5.2 Quantum Thermal Losses

While the energy levels of phonons are in general very far from optical frequencies, the electronic transition frequencies are often within the optical region. When absorption occurs by this method, energy will be re-released at one of the atomic transition frequencies, leading to frequency shift of the field. Another detrimental effect to the integrity of the field stored in the dielectric is that a phase shift will be introduced from the spontaneously emitted photon returning to the field with random phase. If these photons become a significant part of the stored signal, the stored information can be lost.

In the previous section, it was mentioned that the bands of the dispersion diagram are broadened by the losses of the system. This describes the quantum mechanical situation where the states that were originally degenerate are now spread over a range of energies.

When the bands are broadened, phonon transitions may occur within the band. The bandwidth of 2 GHz corresponds to an energy difference of $8 \mu\text{eV}$. A phonon with that energy would have a k vector of 0.46 normalized units, so the energy can be redispersed across the band.

Recall from Chapter 2 that Fermi's Golden Rule has the form:

$$w_k = 2\pi\rho(\omega_k) |\langle i | H_k | f \rangle| \quad (5.11)$$

which can be read as the transition probability is proportional to the density of states times the coupling coefficient between the states. When a transition between the storage state and the propagating state occurs in either of Yanik and Fan structures discussed, the frequency changes are minute, and one can argue that the coupling coefficients between the thermal states to the states in the defect band for the storage state of the structure should be on the order of magnitude to coupling coefficients for the pass-through state of the structure. There is, however, a drastic change in the density of states for the defect bands. As a result, the increased density of states of the storage state cause an approximately proportional increase in the coupling coefficients. This means that in the storage state the interaction with the thermal states will be higher, and the thermal broadening of the stored state will be enhanced.

At first glance, this enhancement of the degeneration of a state stored in a high Q structure may be counterintuitive as such structures are known to have long time constants. However, one should note that the thermal noise coupled into the resonator is also enhanced. Because the coupling in and out of the state is reflexive, electromagnetic states must also easily couple into the thermal states. The long storage time of the resonator and high interaction with the thermal states can be reconciled in the following way: the photon state will generally couple to a phonon nearly the same energy, and a phonon produce a photon with approximately the same energy as well. These transitions will occur at a rate as to nearly cancel, leaving the storage time of the resonator. While the storage time is high, the number of photon-phonon-photon transitions has increased, and each brings a slight change in the frequency content of the stored state. In this way, the state, while being stored longer in the high Q structure, is decohered more quickly from its original state by thermal noise.

The increase in the number of transitions due to the higher density of states, combined with the bandwidth compression each act to enhance the thermal spreading of the stored state. The photon-phonon-photon transition is most likely to occur with very little change in frequency. These transition probabilities decrease exponentially. as the frequency change caused by the transition increases. For the narrower bandwidth signal, this means that the frequencies will be spread further from their original state per photon-phonon-photon interaction. This effect is multiplied by the increased number of these transitions due to the higher Q of the state. In the following section, the equations that describe these interactions will be developed.

5.3 Methodology for Modeling Thermal Interaction

To calculate the evolution of the electromagnetic states, Fermi's Golden Rule was used to generate a finite difference matrix. For each point in the matrix, the transition rate for a single state is multiplied by the density of states to acquire the overall transition rate. For sufficiently small time steps that are much smaller than the transition time, the change in the state can be estimated as being linear in time.

In thermal spreading, the rate of change between two energy levels is dependent upon

the difference between those energy levels is known as the coupling coefficient, $W_{i \rightarrow f}^{(2)}$, which has units of s^{-1} , and can be found to be [16, 31]:

$$W_{i \rightarrow f}^{(2)} = \frac{2\pi}{\hbar} \sum_n \left| \frac{\langle f | H_{per} | n \rangle \langle n | H_{per} | i \rangle}{E_i - E_n} \right|^2 \delta(E_f - E_i) \quad (5.12)$$

where E_i and E_f are the energies of the initial and final states, respectively, and H_{per} is the sum of the interaction Hamiltonians of carrier-photon and carrier-phonon absorption and emissions. The elements of these Hamiltonians have the following forms:

$$\text{carrier phonon abs. } \left| \langle k' | H_{c-pn}^a | k \rangle \right|^2 = |M_q|^2 N_q \delta(k' - k - q) \quad (5.13)$$

$$\text{carrier phonon emis. } \left| \langle k' | H_{c-pn}^e | k \rangle \right|^2 = |M_q|^2 (N_q + 1) \delta(k' - k + q) \quad (5.14)$$

$$\text{carrier photon abs. } \left| \langle k' | H_{c-pt}^a | k \rangle \right|^2 = \frac{\hbar(N_{pt})}{2\epsilon\omega_{pt}V_{pt}} \frac{e^2}{m_0^2} |\langle k' | \hat{e} \cdot p | k \rangle|^2 \delta(k' - k) \quad (5.15)$$

$$\text{carrier photon emis. } \left| \langle k' | H_{c-pt}^e | k \rangle \right|^2 = \frac{\hbar(N_{pt} + 1)}{2\epsilon\omega_{pt}V_{pt}} \frac{e^2}{m_0^2} |\langle k' | \hat{e} \cdot p | k \rangle|^2 \delta(k' - k) \quad (5.16)$$

where $|k\rangle$ and $|k'\rangle$ are the initial and final states, respectively, k and q are the wavevectors of the carriers and phonons, respectively, m_0 is the electron mass, N_q is the phonon population with wavevector q , ϵ is the material permit

The dipole interaction element in Equations 5.15 and 5.16 can be rewritten as follows [31]:

$$|\langle k' | \hat{e} \cdot p | k \rangle|^2 = \frac{m_0^2}{m^{*2}} \hbar^2 (\hat{e} \cdot k)^2 \quad (5.17)$$

where m^* is the carrier's effective mass. The interaction between carriers and phonons or impurities is:

$$\text{polar optical phonon } |M_q|^2 = \frac{e^2 \hbar \omega_{LO} q^2}{2\epsilon_0 (q^2 + q_s^2)^2 V_{pn}} \left(\frac{1}{K_\infty} - \frac{1}{K_S} \right) \quad (5.18)$$

$$\text{deformation pot. optical phonon} = \frac{D_0^2 \hbar^2}{2\rho_L \hbar \omega_0 V_{pn}} \quad (5.19)$$

$$\text{deformation pot. acoustic phonon} = \frac{\Xi^2 \hbar q^2}{2\rho_L \hbar \omega_0 V_{pn}} \quad (5.20)$$

$$\text{piezoelectric acoustic phonon} = \frac{e^2 e_{14}^2 \hbar \omega q^2}{2\epsilon_S^2 \rho_L \nu_s (q^2 + q_s^2)^2 V_{pn}} \quad (5.21)$$

$$\text{charged impurity} = \frac{Z^2 e^4 N_I}{2\epsilon_S^2 (q^2 + q_s^2)^2 V_{pn}} \quad (5.22)$$

where ϵ_0 is the vacuum permittivity, ω_{LO} is the longitudinal optical phonon energy, V_{pn} is the volume of phonon vibration, K_∞ and K_S are the high-frequency and static dielectric constants, respectively, D_0 is the deformation potential for optical phonons, ρ_L is the material density, ω_0 is the angular frequency of the optical phonon, Ξ is the deformation of the acoustic phonons, ω_q is the frequency of the acoustic phonons, ϵ_s is the static dielectric constant of the material, ν_s is the velocity of sound in the material, N_I is the density of the impurity, and Z is ionized charge of the impurity [31]. The static screening wavevector can be calculated as [31]:

$$q_S^2 = \frac{e^2}{\epsilon_S} \frac{\partial n_c}{\partial \mu_{Fc}} \quad (5.23)$$

where n_c is the carrier population density and μ_{Fc} is the quasi-Fermi energy.

There are a total of eight possible phonon-photon interactions: phonon absorption, photon absorption; phonon absorption, photon emission; phonon emission, photon absorption; phonon emission, photon emission; and these interactions with the photon interaction first and the phonon interaction second. Using the nomenclature of $S_{\pm\pm}$ for the product of the Hamiltonian terms phonon emission ($S_{+\pm}$) and absorption ($S_{-\pm}$), and photon emission ($S_{\pm+}$) and absorption ($S_{\pm-}$). These terms simplify to [31]:

$$|S_{++}|^2 = |S_{+-}|^2 = |M_q|^2 N_q \frac{\hbar N_{pt} e^2}{2\epsilon\omega_{pt}^2 V_{pt} m^{*2}} (\hat{e} \cdot q)^2 \quad (5.24)$$

$$|S_{--}|^2 = |S_{-+}|^2 = |M_q|^2 (N_q + 1) \frac{\hbar N_{pt} e^2}{2\epsilon\omega_{pt}^2 V_{pt} m^{*2}} (\hat{e} \cdot q)^2 \quad (5.25)$$

The coefficient of free-carrier absorption is the net change in the quantity of photons:

$$\alpha_{fca} \equiv \frac{V_{pt}}{\nu_g N_{pt} V_c} \sum_k W_{k \rightarrow k \pm q} f_k (1 - f_{k \pm q}) \quad (5.26)$$

where ν_g is the group velocity of the photons, f_k is the carrier distribution function corresponding to wavevector k , and $f_k(1 - f_{k \pm q})$ is the carrier distribution factor representing the initial available states and the final unblocking states [31].

Assuming parabolic energy level valleys and intravalley transitions, this results in the following equation for the free-carrier absorption coefficient:

$$\begin{aligned}
\alpha_{fca} &= \frac{e^2 k_B T_c}{12\pi^3 \epsilon_0 n_r c \omega_{pt}^3 \hbar^4} \int_0^\infty dq q^3 V_{pn} |M_q|^2 \\
&\times \left\{ \frac{N_q}{\exp(-\varepsilon_q - \varepsilon_{pt}) - 1} \ln \left[\frac{1 + \exp(\eta - \varepsilon_q - \varepsilon_{pt} - \varepsilon_{--}^{min})}{1 + \exp(\eta - \varepsilon_{--}^{min})} \right] \right. \\
&\quad + \frac{N_q + 1}{\exp(\varepsilon_q - \varepsilon_{pt}) - 1} \ln \left[\frac{1 + \exp(\eta + \varepsilon_q - \varepsilon_{pt} - \varepsilon_{+-}^{min})}{1 + \exp(\eta - \varepsilon_{+-}^{min})} \right] \\
&\quad - \frac{N_q}{\exp(-\varepsilon_q + \varepsilon_{pt}) - 1} \ln \left[\frac{1 + \exp(\eta - \varepsilon_q + \varepsilon_{pt} - \varepsilon_{-+}^{min})}{1 + \exp(\eta - \varepsilon_{-+}^{min})} \right] \\
&\quad \left. - \frac{N_q + 1}{\exp(\varepsilon_q + \varepsilon_{pt}) - 1} \ln \left[\frac{1 + \exp(\eta + \varepsilon_q + \varepsilon_{pt} - \varepsilon_{++}^{min})}{1 + \exp(\eta - \varepsilon_{++}^{min})} \right] \right\}
\end{aligned} \tag{5.27}$$

where

$$\begin{aligned}
\varepsilon_q &= \hbar\omega_q/k_B T_c \\
\varepsilon_{pt} &= \hbar\omega_{pt}/k_B T_c \\
\varepsilon_{\pm\pm}^{min} &= \hbar^2 (k_{\pm\pm}^{min})^2 / 2m^* k_B T \\
k_{\pm\pm}^{min} &= |q/2 + m^*(\pm\omega_q \pm \omega_{pt})/\hbar q| \\
\eta &= \mu_{Fc}/k_B T_c
\end{aligned} \tag{5.28}$$

$\omega_q = \omega_{LO}$ for LO phonons, $\omega_q \approx \nu_s q$ for acoustic phonons, $\omega_q = 0$ for charge impurity T_c is the carrier temperature, which may be different from the temperature of the material lattice.

Intervalley transitions dominate when the energy of the photons exceeds the difference between the energy level valleys [31]. Because the energy of the photons used in telecommunications are in the range of 0.8 eV to 1.0 eV, while the difference between the depths of energy level valleys in the conduction band of gallium arsenide is 0.3 eV [3], intervalley transitions will be the dominant interaction between carriers, phonons, and photons. The intervalley absorption coefficient for free-carrier absorption is [31]:

$$\begin{aligned}
\alpha_{fca} &= \frac{e^2 k_B T_c}{12\pi^3 \epsilon_0 n_r c \omega_{pt}^3 \hbar^4} \int_0^\infty dq q^3 V_{pn} |M_q|^2 \\
&\times \left\{ \frac{N_q}{\exp(-\varepsilon_q - \varepsilon_{pt}) - 1} \ln \left[\frac{\exp(-\eta + \varepsilon_q + \varepsilon_{pt}) + \exp(-\varepsilon_{--}^{min})}{\exp(-\eta + \varepsilon_q + \varepsilon_{pt}) + \exp(-\varepsilon_{--}^{max})} \frac{\exp(-\eta) + \exp(-\varepsilon_{--}^{max})}{\exp(-\eta) + \exp(-\varepsilon_{--}^{min})} \right] \right\}
\end{aligned} \tag{5.29}$$

$$\begin{aligned}
& + \frac{N_q + 1}{\exp(\varepsilon_q - \varepsilon_{pt}) - 1} \ln \left[\frac{\exp(-\eta - \varepsilon_q + \varepsilon_{pt}) + \exp(-\varepsilon_{+-}^{min})}{\exp(-\eta - \varepsilon_q + \varepsilon_{pt}) + \exp(-\varepsilon_{+-}^{max})} \frac{\exp(-\eta) + \exp(-\varepsilon_{+-}^{max})}{\exp(-\eta) + \exp(-\varepsilon_{+-}^{min})} \right] \\
& - \frac{N_q}{\exp(-\varepsilon_q + \varepsilon_{pt}) - 1} \ln \left[\frac{\exp(-\eta + \varepsilon_q - \varepsilon_{pt}) + \exp(-\varepsilon_{-+}^{min})}{\exp(-\eta + \varepsilon_q - \varepsilon_{pt}) + \exp(-\varepsilon_{-+}^{max})} \frac{\exp(-\eta) + \exp(-\varepsilon_{-+}^{max})}{\exp(-\eta) + \exp(-\varepsilon_{-+}^{min})} \right] \\
& - \frac{N_q + 1}{\exp(\varepsilon_q + \varepsilon_{pt}) - 1} \ln \left[\frac{\exp(-\eta + \varepsilon_q + \varepsilon_{pt}) + \exp(-\varepsilon_{++}^{min})}{\exp(-\eta + \varepsilon_q + \varepsilon_{pt}) + \exp(-\varepsilon_{++}^{max})} \frac{\exp(-\eta) + \exp(-\varepsilon_{++}^{max})}{\exp(-\eta) + \exp(-\varepsilon_{++}^{min})} \right] \Big\}
\end{aligned}$$

where, in addition to the previously defined quantities:

$$\begin{aligned}
\varepsilon_{\pm\pm}^{max} &= \hbar^2 (k_{\pm\pm}^{max})^2 / 2m^* k_B T & (5.30) \\
k_{\pm\pm}^{max} &= |(1 + \sqrt{1 - 4ab_{\pm\pm}}) / 2a| \\
k_{\pm\pm}^{min} &= |(1 - \sqrt{1 - 4ab_{\pm\pm}}) / 2a| \\
a &= (1 - m_j^* / m_i^*) / 2q \\
b_{\pm\pm} &= q/2 + m_j^* E_{\pm\pm}^{ji} / \hbar^2 q \\
E_{\pm\pm}^{ji} &= \pm \hbar \omega_q \pm \hbar \omega_{pt} + E_j - E_i \\
|M_q|^2 &= \frac{D_{ij}^2 \hbar^2}{2\rho_L \hbar \omega_{ij} V_{pn}}
\end{aligned}$$

Note that $k_{\pm\pm}^{min}$ has been generalized for the intervalley case and that the i and j index the valley to which the value corresponds, D_{ij} is the intervalley deformation potential and ω_{ij} is the frequency of the phonon involved in the interaction. Table 5.1 summarizes the relevant properties for gallium arsenide used to calculate the absorption and coupling coefficients [3, 31].

The calculations were performed for a lattice temperature and carrier temperature of 300 kelvin. Assumptions made to simplify calculation are that polarized optical phonons and deformation acoustic phonons dominate [31], and that piezoelectric effect is negligible. Only carriers in the X and L valleys will interact with deformation potential phonons. [31]

Near the band edge, the density of electronic states is [19]:

$$g(E) = \frac{\sqrt{2m^*(E - E_\Gamma)}}{\pi^2 \hbar^3} \quad (5.31)$$

When the photon energy is greater than the difference in conduction band valleys, intervalley phonons dominate [31]. Wavelengths used in optical communications have sufficient energy to excite intervalley phonons in gallium arsenide. In such a case, intravalley phonons can be ignored.

Property	Symbol	Value	Units
Effective Mass of Electron in Γ valley	$[m_e^\Gamma]$	0.067	m_0
Effective Mass of Electron in L valley	$[m_e^L]$	0.55	m_0
Effective Mass of Electron in X valley	$[m_e^X]$	0.85	m_0
$L - \Gamma$ Energy Difference	$[E_L - E_\Gamma]$	0.284	eV
$X - \Gamma$ Energy Difference	$[E_X - E_\Gamma]$	0.476	eV
Band Gap	$[E_G]$	1.424	eV
Fermi Energy Level	$[\mu_{Fc}]$	0.712	eV
LO Phonon Energy	$\hbar\omega_{LO}$	36.25	meV
TO Phonon Energy	$\hbar\omega_{TO}$	33.29	meV
Static Dielectric Constant	K_S	13.18	–
High-Frequency Dielectric Constant	K_∞	10.89	–
Optical Phonon Deformation Potential	D_0	$3.5 \cdot 10^{10}$	eV/m
Acoustic Phonon Deformation Potential	Ξ	6.7	eV
Piezoelectric Constant	e_{14}	–.16	C/m
Velocity of Sound	ν_s	$4 \cdot 10^3$	m/s
Material Density	ρ_L	$5.36 \cdot 10^3$	kg/m^3
Intervalley Deformation Potential	$D_{\Gamma L/X}$	10^{11}	eV/m
$\Gamma - L$ Intervalley Deformation Phonon	$\hbar\omega_{\Gamma L}$	27.8	meV
$\Gamma - X$ Intervalley Deformation Phonon	$\hbar\omega_{\Gamma X}$	29.9	meV

Table 5.1: Material Properties for Gallium Arsenide

Once the carriers have been excited, they may return to the ground state by either spontaneous emission of a photon or by stimulated emission because of the stored field. The coefficient for emission is the carrier -photon emission coefficient in Equation 5.16 above. The energy of the carrier will be reduced by $\hbar\omega_{pt}$, while the change in the momentum of the carrier will be negligible.

In a single time step, the photon is will be found in its initial state with a probability of $e^{-\frac{\Delta t}{\tau}}$ where Δt is the time step, and τ is the life of the electromagnetic state in the

material as discussed earlier. For sufficiently small time steps, this equation can be reduced to $1 - \frac{\Delta t}{\tau}$. This result is used as the diagonal matrix elements.

When one assumes Drude conductivity, the absorption factor for an intrinsic semiconductor is [24]: $\alpha_{fca} = \frac{e^3 \lambda^2 n_i}{4\pi^2 K_S \epsilon_0 c^3 m^{*2} \mu}$. While Tsai et al. showed that the Drude model has errors as high as a two to one ratio, It may be used to predict the order of magnitude of the losses. Drude conductivity will not predict the coupling into the carrier and phonon modes, and quantum coupling coefficients will be needed to describe these effects.

5.4 Implementation of Algorithm

This section describes the algorithm implemented in MATLAB. Assumptions made for the MATLAB calculations were that the wavelength of the signal is 1550 nm, and the lattice constant is 593.835 nm. The duration of the bandwidth compression is one nanosecond.

First, the coefficients for Equations 5.18 through 5.28 that are independent of photon energy and carrier energy were calculated. The carrier states were calculated, and the coupling coefficients between the photon states and carrier states as per Equation 5.16 were found and inserted into a coupling coefficient matrix. This is accomplished by using a nested loop which calculates each coefficient for each photon and carrier energy bin and inserts it into the matrix. The delta function in the equation is implemented by filling the matrix element if the difference within the delta function is less than or equal to the photon energy step size. The calculations are performed for phonon energies from zero to the energy of the TO phonon. This matrix was used to account for the spontaneous emission of photons at each time step.

Next, a matrix for the phonon-photon interactions was generated in a similar fashion based on Equation 5.29. In each loop iteration, the coefficients in Equation 5.30 are calculated and used to determine the matrix element of the phonon-photon coupling matrix.

Next, the time evolution of the field is determined. The transition from the open state to the storage state is calculated without losses as the time of this transition is expected to be much shorter than the time for which losses will occur. The Euler method is used to determine the solution numerically [6]. For a given differential equation, the Euler method

has the form:

$$y(t + \Delta t) \approx y(t) + y'(t) \cdot \Delta t \quad (5.32)$$

If the time step is sufficiently small, in the case of the MATLAB script, 10 picoseconds was chosen, which was less than 0.1 percent of the simulation time, and approximately 0.2 percent of the expected decay time constant of the system.

Because $y'(t)$ is a linear function of $y(t)$, the system can be reduced to

$$\mathbf{Y}(t + \Delta t) \approx \mathbf{Y}(t) + \mathbf{H} \cdot \mathbf{Y}(t) \cdot \Delta t = [\mathbf{I} + \mathbf{H} \cdot \Delta t] \cdot \mathbf{Y}(t) \quad (5.33)$$

In the case of no cross coupling between frequencies, this matrix would simply be

$$\mathbf{A} = \mathbf{I} \cdot (1 - \alpha_{fca} \cdot v_p \cdot \Delta t) \quad (5.34)$$

This matrix is expanded to include the interaction between the carriers and the stored field

$$\mathbf{A}_{exp} = \begin{bmatrix} \mathbf{A} & \mathbf{H} \\ \mathbf{H}^\dagger & \mathbf{I} \end{bmatrix} \quad (5.35)$$

In the final version of the MATLAB script, the change to the carrier state was assumed to be negligible, while the carriers did effect the stored field.

5.5 Results from Simulation of Yanik and Fan structure

The algorithm from the previous section was implemented in MATLAB. First, the energy distribution of the carriers was calculated. This result can be seen in Figure 5.1. This distribution is as expected for a semiconductor in that there are no carriers in the band gap and that the carrier density is highest near the band gap.

At this point, let us discuss how these interactions will result in the loss of the coherent state in the Yanik and Fan structure. In the fast moving state, not much light is absorbed as the wave propagates through due to the relatively short time of the interaction. During the adiabatic transition of the waveguide, the bandwidth of the signal is compressed and the density of states increases. The amplitude of the signal and the noise increase as a

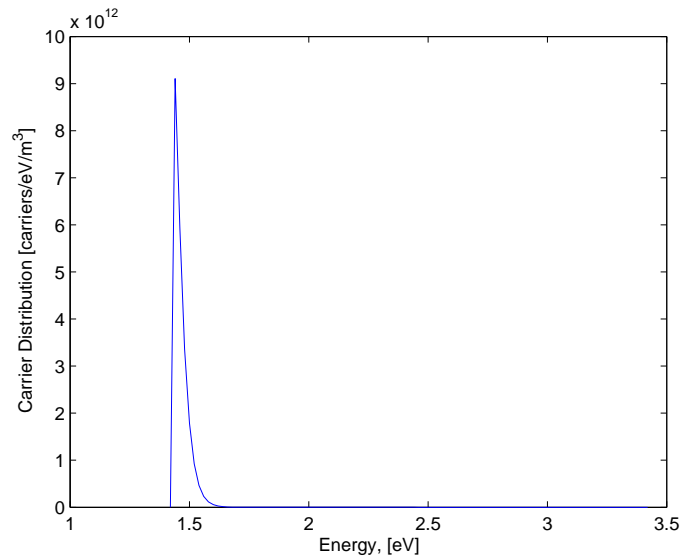


Figure 5.1: Carrier Distribution in Gallium Arsenide at 300K

consequence. As the coherent light is absorbed by the material, it is redistributed over the allowed states. The distribution will approach thermal equilibrium, and the states will be filled according to the density of states.

Because the energy will be stored in a high Q state in the band gap, the states will transition between each other with increased probability. As a result, as the energy from the stored state is dissipated, it is redistributed over the high Q band holding the stored state. When the bandwidth is restored for the state, the redistributed energies are expanded along with the signal.

The time constant for rate at which the signal is lost is $\frac{Q}{\omega}$. In the case of a 200 THz signal in gallium arsenide, this time constant is approximately 5 nanoseconds. Because the density of states of the bands in the band gap are almost double the density of states elsewhere in the spectrum, most of the energy is redistributed into these bands. Because of this, the information in the band is lost faster than it would be if it had simply had fallen below a static noise floor, as seen in Figures 5.2 and 5.3. In these figures, MATLAB has implemented the decay rates and spreading from above. The result is that the information

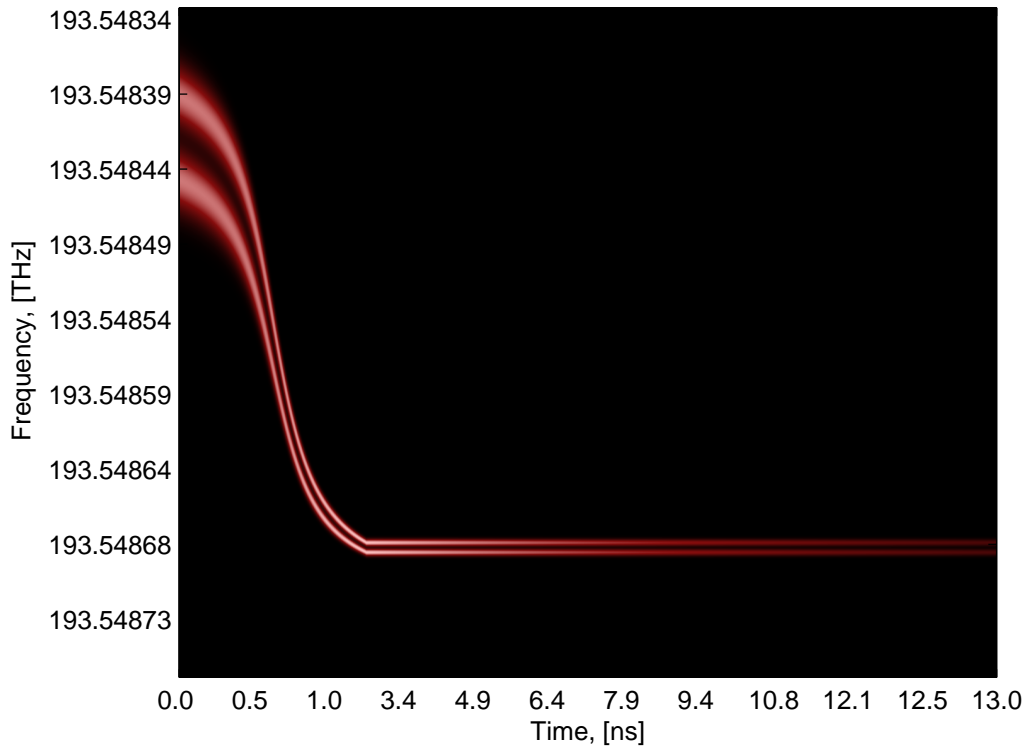


Figure 5.2: Thermal Interaction with the Compressed State.

in the signal is essentially lost if the duration is greater than 10 nanoseconds for the situation outlined above.

As seen in Figure 5.3, the loss in magnitude of the signal was nearly 20 dB, which is nearly what is to be expected when storing a signal for two time constants. While a signal which has decreased by 20 dB is often recoverable, the effective increase in noise reduces the signal to noise ratio to only 6 dB makes recovery of the signal more difficult, and if the storage time is doubled, the signal will be completely buried in the noise.

Figure 5.4 illustrates the percent difference between the signal with thermal spreading accounted for versus what the signal would look like with simple attenuation. Beyond the edges of the signal, the difference climbs rapidly as thermal spreading adds energy to frequencies where much less energy was present in the original signal. Between the two

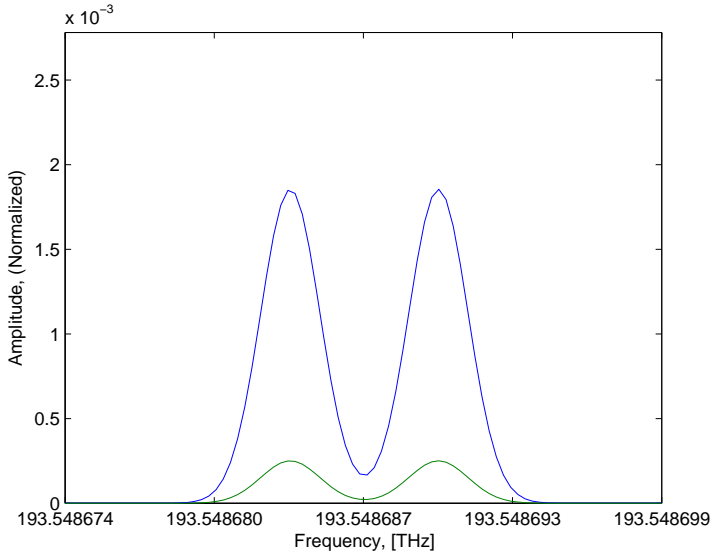


Figure 5.3: Deterioration of Signal in Stored State, Including Effects Due to Thermal Field

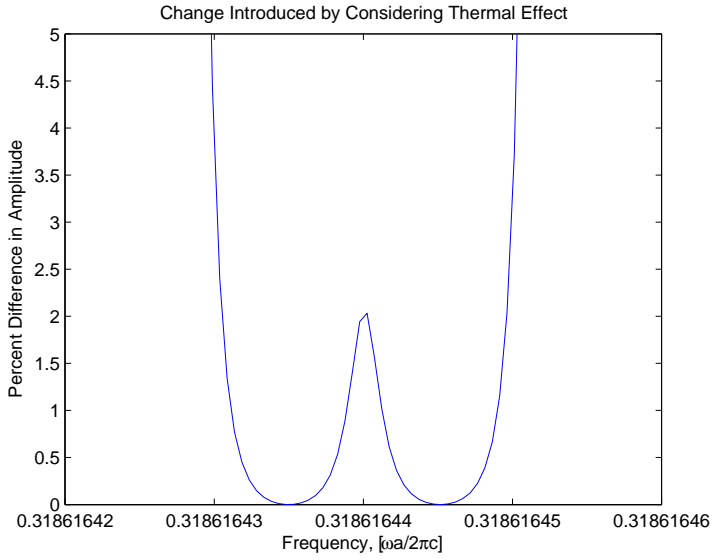


Figure 5.4: Percent Difference between Signal with Thermal Spreading and without Thermal Spreading

peaks, the signal level increases by two percent.

Chapter 6

Conclusions

The tasks performed in completion of this thesis are as follows:

1. The electric field was simulated for a single resonator CROW structure, and the coupling coefficients between resonators was calculated using MPB to solve Maxwell's Equations and MATLAB to analyze the data.
2. The electric field was also found in MPB for two versions of the Yanik and Fan structure in both the storage and propagating states to acquire the mode shapes, propagation velocities, and other properties for each of the structures.
3. The local density of states was calculated numerically, again using MPB and MATLAB, in order to calculate coupling coefficients for interactions with thermal states.
4. A model for the evolution of the electromagnetic state due to interaction with the thermal field was implemented and the data were analyzed.

The Yanik and Fan structure essentially converts between being a waveguide and being a high Q resonator. This allows it to accept a state and store it without waveguide dispersion. Loss mechanisms in the material allow this state to decay to thermal equilibrium. In the stored state, the field is vulnerable to phonons that can change their momentum, which smears the spectrum, however, this smearing is nearly negligible.

One measure of the severity of the smearing is if one considers the double hump structure to be three OFDM "bins", one may note that the input signal has approximately 20 dB

of difference (10:1 ratio) between the peaks and central trough. the output signal has a difference of 19.6 dB. Most communication systems separate symbols by 3 dB or more, so this difference is negligible.

The results gathered from the numerical analysis produced very high Q states, some of which have not yet been realized in photonic crystals. The analysis in [35] had not accounted for defects in the placement, shape, or index, all of which contribute to scattering losses.

In the storage state, the Yanik and Fan structure is essentially a optical resonator cavity. Cavities have been well studied for their quantum effects [1, 16]. As with other resonators the CROW and by extension, the Yanik and Fan structure preserves the quantum state until the state is absorbed into the thermal field.

The inherent losses within a dielectric material due to the thermal field are enhanced in the case of the Yanik and Fan structure by the bandwidth compression. Higher compression leads lower waveguide dispersion, however higher losses due to the thermal field interactions will occur.

Losses due to the absorption coefficient is the dominant mechanism at 300K. This effect grows rapidly as temperature increases because intrinsic carrier concentration increases exponentially with temperature [19]. The noise floor also increases with increasing temperature. These effects result in the storage time decreasing significantly with increasing temperature. One basis for future work is accounting for cases where the signal is a significant portion of energy stored in the structure, such that it appreciably disturbs the carrier state or the phonon state of the material.

There are a number of options to mitigate the losses and improve the performance of the system. First, base materials with the lowest possible conduction should be used. Because of the relatively narrow band-gap of gallium arsenide compared to more insulative materials, the conduction is not negligible; more insulative materials should be used. The crystal should also be free from defects to reduce the presence of R-G recombination centers [19]. In some cases it may be an option to reduce losses by cooling the structure. In semiconductors such as gallium arsenide, one may use PN junctions to create a thermoelectric cooler to cool only the area needed.

Lower loss structures may also be used; for example, if the CROW structure can be made up of ring resonators. The ring resonator described in [11] has a quality factor of about 10^8 which would allow the state to be stored for on the order of a microsecond. The final option to preserve the stored state is to use a gain medium to enhance the stored field via stimulated emission. Barring these methods, the time stored in a bandwidth compressed state must be limited to prevent loss of the stored state due to interaction with the thermal field. In the case studied in this thesis, the storage time of the state must be limited to approximately 10 nanoseconds in order to be able to recover the stored state.

The use of photonic crystals to realize logic and delay structures has driven the imagination of researchers. Practical optical logic circuits seem mere inches from grasp, and Yanik and Fan's delay structure may be at the heart of such systems as they arrive.

Appendix A

Thermal Simulation MATLAB Script

```

% Thermal spreading: New Finite difference model
% Based on Tsai et al coefficients
% Eduardo Oliveira
% July 26, 2007 (based on earlier code from 2006)

clear all;
%variables (all MKS units)
n      = 1e-9;      %nano
u      = 1e-6;      %micro
c      = 3e+8;      %Speed of light in a vacuum [m/s]
ec     = 1.602e-19; %electron charge [C]
m_0    = 9.11e-31; %electron mass [kg]
T      = 300;      %lattice temperature [K] ***add to assumptions
Tc     = 300;      %carrier temperature [K]
kB     = 8.6173e-5*ec; %Boltzmann's constant [J/K]=[eV*ec/K]
EGam   = 1.42*ec;  %Energy of Gamma valley [J]=[eV*ec]
EX     = 1.90*ec;  %Energy of Gamma valley [J]=[eV*ec]
EL     = 1.78*ec;  %Energy of Gamma valley [J]=[eV*ec]

muFc   = 0.712*ec; %Fermi energy level [J]=[eV*ec]
m_eGam = 0.067*m_0; %Gamma electron effective carrier mass [kg]
m_eL   = 0.55*m_0; %L electron effective carrier mass [kg]
m_eX   = 0.85*m_0; %X electron effective carrier mass [kg]

LOphon = 0.03625*ec; %LO phonon energy [J]=[eV*ec]
TOphon = 0.03329*ec; %TO phonon energy [J]=[eV*ec]

```

```

epselec =8.85418e-12;%Permittivity of free space [F/m]
Kopt    =12.00;      %Optical dielectric constant
KS      =13.18;      %Static dielectric constant
Kinf    =10.89;      %High freq. dielectric constant
D0      =3.5e10*ec;  %Optical Phonon Deformation Potential [J/m]=[eV*ec/m]
Xi      =6.7*ec;     %Acoustic Phonon Deformation Potential [J]=[eV*ec]
e14     =-0.16;     %Piezoelectric Constant [C/m]
DGamX   =1e11*ec;   %Intervalley Deformation Potential [J/m]=[eV*ec/m]
DGamL   =1e11*ec;   %Intervalley Deformation Potential [J/m]=[eV*ec/m]
hbomGamX=0.0278*ec; %GamL Intervalley Deformation Pot phonon [J]=[eV*ec]
hbomGamL=0.0299*ec; %GamX Intervalley Deformation Pot phonon [J]=[eV*ec]
hbar    =6.6261e-34/2/pi; %reduced planck's constant [J*s]
nu_s    =4e3;       %speed of sound [m/s]
rho_L   =5.36e3;    %material density [kg*m^-3]

qpnmax=T0phon/hbar/nu_s;%[m^-1] assuming phonon energies up to T0 phonons
qpnstep=qpnmax/100; %[m^-1]

qphon=qpnstep:qpnstep:qpnmax;%[m^-1] fixed 8/6/07
omega_q=nu_s*qphon;%[Hz] fixed 8/3/07,fixed again 8/6/07
epsq=hbar*omega_q/(kB*T);%[J/J]
aX =(1-m_eX/m_eGam)/2./qphon;%[m] %assumes Gam-X transitions dominate
aL =(1-m_eL/m_eGam)/2/ec;%[m]
aGam = 0;%[m]

basef=200e+12;%the actual frequency in Hz
Q=10^5;%Q of resonator
omegadiff=2*pi*.0000000005;%dimensionless frequency step
X=(.3186158:omegadiff/2/pi:.3186166)';%dimensionless freq range

%plot(X,exp(-((X-.3155).^2)/(2*.0001^2)))
%width0 = .00007;%sqrt(2)*sigma of incoming pulse

%spreading = width0*t*u;

%true inputs
f1=.3186159;%lower gaussian cf input old:%f1=.3157;%lower gaussian cf input
f2=.3186160;%upper gaussian cf input old:%f2=.3162;%upper gaussian cf input
width0 = .00000002;%sqrt(2)*sigma of incoming pulse

%loss based inputs
tau = .5e-8;%rate of drop in height
tau2 = 3e-8;%rate of spreading

```

```

%compression based inputs (from mpb)
shiftfactor = n/6;
squeezefactor = n/6;
cff = .3186165; %stored center frequency

%computation*****
width=width0;
cf =(f1+f2)/2; %input center frequency
fplus = f2-cf; %upper sideband distance
fminus = f1-cf; %lower sideband distance
delcf = cf-cff;
peak1 = 1e16;%photons??ns burst at 1.23e14 rad/sec, total energy stored =??

%assumptions and input data/variables
lambdain =1550*n; %wavelength of the band operated at [m]
Vpn =pi*(10*lambdain/.3186159)^3;%[m^3]Phonon interaction volume
%fixed!8/10

estep = 0.02*ec; %energy stepsize for carriers [J]
elecenergies= 1.42*ec:estep:3.42*ec;%1.42eV - 3.42 eV, 2 meV steps [J]
states =120; %states in single mpb bin in question**
mpbstep =.38/640000; %freq bin size from mpb**
t12jnt =2e-9; %time that storage starts [s]
tstep2 =1e-11; % temporary time step [s]
t23jnt =t12jnt+tstep2*1000;%return from compressed state start time[s]
t2=t12jnt:tstep2:t23jnt; %storage time vector [s]

%calcs based on assumptions
a =lambdain*cf; %lattice spacing in [m]
Vpt =10*a^3; %[m^3] Photon interaction volume
% assumes rods are ~10*a tall
omega_pt =X*2*pi*c/a; %unnormalized input frequencies [rad/s]
delomega_pt =omega_pt(2)-omega_pt(1);%frequency spacing
kc =sqrt(2*m_eX*elecenergies)/hbar;%[m^-1]
%carrier wavenumber ass X valley
emstep =omegadiff*c/a; %EM frequency spacing [Hz]
dosem =states/mpbstep/emstep; %assume nearly linear dE/dk nearby
%should be 1/Hz, 1/(m^3)/Hz, or 1/(m^3)/J

% Make Coefficients
MqsqGamX=DGamX^2*hbar^2/(2*rho_L*hbomGamX*Vpn); %GamX Interval coeff [J^2]
MqsqGamL=DGamL^2*hbar^2/(2*rho_L*hbomGamL*Vpn); %GamL Interval coeff [J^2]
eta=muFc/(kB*Tc); %[J/J]
epsqL0 = L0phon / (kB*Tc); %[J/J]

```

```

%epsqA = nus*q;%function of q
%epspt=function of photon energy

%%below was commented, shows initial graph of input
%%Y=exp(-((X-cf1).^2)/(2*width^2))+exp(-((X-cf2).^2)/(2*width^2));
%Y=peak*(exp(-((X-(cf+fplus)).^2)/(2*(width)^2))...
%      +exp(-((X-(cf+fminus)).^2)/(2*(width)^2)));
%figure(1)
%plot(X,Y)
%%**end

%Bandwidth compression simulation based on MPB:
numtstep1=300;
t1end=1e-9;
% bandwidth compression
t=0:(t1end/numtstep1):t1end;
matrix=zeros(length(omega_pt),(numtstep1+length(t2)));
carrmat=[];
for en=1:numtstep1%increase to show compression
    shift =atan((t(en)-.5*n)/shiftfactor)/pi*delcf+.5*delcf;
    squeeze=.5-atan((t(en)-.5*n)/squeezefactor)/pi;
    peak= peak1*exp(-t(en)/tau);
    %shift = t(en)/n*.01;
    %peak/squeeze was peak
    pk1= peak/(squeeze)^(.25);
    matrix(:,en)=pk1*hbar*omega_pt.*...
        (exp(-((X-(cf+fplus*squeeze-shift)).^2)/(2*(width*squeeze)^2))...
        +exp(-((X-(cf+fminus*squeeze-shift)).^2)/(2*(width*squeeze)^2)));
    encarry = en;
end
entoo = encarry; %used to store/find the end of the squeezing

% Setup Finite difference matrix

%t2=2e-9:3e-11:2e-8;%bad, just for testing
matrix1= matrix(:,encarry);%First row going in to time evolution

nx= length(matrix1);
%load initial carrier state
% number of carriers = Carrier dos* exp((Ek-muFc)/(kB*Tc))^-1
elecDos = estep*sqrt(2*(m_eGam)^3*(elecenergies-EGam))/pi^2/hbar^3;%[m^-3]
%fixed 8/9/07

```

```

fermifunc = 1./(1+exp((elecenergies-muFc)/kB/Tc));
carrierstate = (elecDos.*fermifunc)';%[m^-3]
tempvect = carrierstate;
carrierst1 = (elecenergies-EGam)'.*carrierstate;
%plot(elecenergies/ec,carrierstate)%for debugging.

%carrier lifetime = 2*pi/hbar*integral(W(f,i)'*W(f,i)*photonic dos)
%W(f,i)=
%<k'|H_{cpt}|k>=
Hcpt=zeros(length(kc),length(omega_pt));

for ind1=1:length(kc)
    for ind2=1:length(omega_pt)
        %Hcpt(ind1,ind2)=hbar^3*dosem*ec^2/(2*Kopt*epselec*...
        %    omega_pt(ind2)*(m_eX)^2)*(kc(ind1)/2)^2;%fixed 8/4/07
        if abs(elecenergies(ind1)-hbar*omega_pt(ind2))<=delomega_pt
            %are we dirac(0), within the granularity of the matrix?
            Hcpt(ind1,ind2)=sqrt(hbar^3*ec^2/(Vpt*2*Kopt*epselec*...
                omega_pt(ind2)*((m_eX)^2+(m_eL)^2))*(kc(ind1)/2)^2);%[J]
            %Hcpt(ind1,ind2)=sqrt(hbar^3*ec^2/(Vpt*2*Kopt*epselec*...
            %    omega_pt(ind2)*(m_eX)^2)*(kc(ind1)/2)^2);%[J]
            %dosem should be Npt, which will vary!!!, the good news is
            %one only needs to factor it out and multiply by sqrt(Npt)
            %in the loop*****Npt replaced by 1 for spontaneous
            %emission
        end
    end
end
pcd = Hcpt*tstep2/hbar;%fixed 8/4/07,8/10/07 [s/s],coupling coef per step
        %\Delta{y}/\Delta{t}=-R*y

%using linear relationship between omega and k for photons because we are
%assuming compression was big enough for linearization
%may be slightly inaccurate here, not sure which carrier mass to use,
%assuming m_eX due to dominance of intervalley transitions due to photon
%energy. Largest mass, it will tend to underestimate coupling carrier
%momentum will not change significantly in the transition
%half the momenta will be aligned with the photons, thus the factor of 1/2
%in the kc term

% "A" matrix contains electromagnetic decay (photon-carrier-phonon)
%probs(freq/Energy domain)

%format:

```

```

%A1=
%[(electro-      (photon-   ]
%[ magnetic      carrier    ]
%[ state decays) coeffs)    ]
%%%%%%%%%%%%%%%%%%%%%%%%%%%%%%%%%%%%%%%%%%%%%%%%%%%%%%%%%%%%%%%%%%%%%%%%
%A2=
%[(photon-      carrier-    ]%should this be carrier-phonon?
%[carrier        carrier    ]
%[ coeffs)       interactions]

%Sppsqs=
%Spmsqs=Sppsqs;

Hptcpn=zeros(length(kc),length(omega_pt));
alphaconst = ec^2*kB*Tc*Q/(12*pi^3*epselec*Kopt*hbar^4);%[kg^-2*m^-3]vg=c/Q
%A = spdiags(vv,-qty:qty,nx,nx); %spdiags=old method!!
tmpdata=[];

%Generate coupling coefficients
preHptcpn=zeros(length(kc),length(omega_pt));

for inda=1:length(kc)
    fprintf('.')
    if(~mod(inda,40))
        fprintf('\n');
    end
    for indb=1:length(omega_pt)
        epspt=hbar*omega_pt(indb)/(kB*Tc);%[J/J] chkd 8/3/07
        %for qphon=T0phon/100:T0phon/100:T0phon
        EXGampp = +hbar*omega_q+hbar*omega_pt(indb)+EX-EGam; %[J]
        %ELGampp = +hbar*omega_q+hbar*omega_pt(indb)+EL-EGam; %[J]
        bXpp = qphon/2+m_eX*EXGampp./(hbar^2*qphon);%[m^-1]
        %bLpp = qphon/2+m_eX*ELGampp./(hbar^2*qphon);%[m^-1]

        kminpp = abs(1-sqrt(1-4.*aX.*bXpp)/2./aX);%[m^-1]
        kmaxpp = abs(1+sqrt(1-4.*aX.*bXpp)/2./aX);%[m^-1]
        %kmaxpp=abs(qphon/2+m_eX*m_0*(hbar*(nu_s*qphon+omega_pt(indb)))...
        %    /(hbar^2*qphon));%*****
        exppp=exp(-eta+epsq+epspt);%[dimensionless]
        expeminpp=exp(-hbar^2*kminpp.^2/(2*m_eGam*kB*Tc));%[-] assmd m_eGam
        expemaxpp=exp(-hbar^2*kmaxpp.^2/(2*m_eGam*kB*Tc));%[-] assmd m_eGam
        %expemaxpp=0;%*****
        logpp=log((exppp+expeminpp).*(exp(-eta)+exp(expemaxpp))./...

```

```

((exppp+expemaxpp).*(exp(-eta)+exp(expeminpp))))...
./(exp(-epsq-epspt)-1);%checked ok 8/2/07

EXGampm = +hbar*omega_q-hbar*omega_pt(indb)+EX-EGam;%[J]
bXpm = qphon/2+m_eX*EXGampm./(hbar^2*qphon);%[m^-1]
kminpm = abs(1-sqrt(1-4.*aX.*bXpm)/2./aX);%[m^-1]
kmaxpm = abs(1+sqrt(1-4.*aX.*bXpm)/2./aX);%[m^-1]
%kmaxpm=abs(qphon/2+m_eX*m_0*(hbar*(nu_s*qphon+omega_pt(indb))))...
%    /(hbar^2*qphon);%*****
exppm=exp(-eta-epsq+epspt);%[dimensionless]
expeminpm=exp(-hbar^2*kminpm.^2/(2*m_eGam*kB*Tc));%[-] assmd m_eGam
expemaxpm=exp(-hbar^2*kmaxpm.^2/(2*m_eGam*kB*Tc));%[-] assmd m_eGam
%expemaxpm=0;%*****
logpm=log((exppm+expeminpm).*(exp(-eta)+exp(expemaxpm)))/...
((exppm+expemaxpm).*(exp(-eta)+exp(expeminpm))))...
./(exp(-epsq-epspt)-1);%[-] checked 8/2/07

EXGampp = -hbar*omega_q+hbar*omega_pt(indb)+EX-EGam;%[J]
bXmp = qphon/2+m_eX*EXGampp./(hbar^2*qphon);%[m^-1]
kminmp = abs(1-sqrt(1-4.*aX.*bXmp)/2./aX);%[m^-1]
kmaxmp = abs(1+sqrt(1-4.*aX.*bXmp)/2./aX);%[m^-1]
%kmaxmp=abs(qphon/2+m_eX*m_0*(hbar*(nu_s*qphon+omega_pt(indb))))...
%    /(hbar^2*qphon);%*****
expmp=exp(-eta+epsq-epspt);%[dimensionless]
expeminmp=exp(-hbar^2*kminmp.^2/(2*m_eGam*kB*Tc));%[-] assmd m_eGam
expemaxmp=exp(-hbar^2*kmaxmp.^2/(2*m_eGam*kB*Tc));%[-] assmd m_eGam
%expemaxmp=0;%*****
logmp=log((expmp+expeminmp).*(exp(-eta)+exp(expemaxmp)))/...
((expmp+expemaxmp).*(exp(-eta)+exp(expeminmp))))...
./(exp(-epsq-epspt)-1);%[-] checked 8/2/07

EXGamm = -hbar*omega_q-hbar*omega_pt(indb)+EX-EGam;%[J]
bXmm = qphon/2+m_eX*EXGamm./(hbar^2*qphon);%[m^-1]
kminmm = abs(1-sqrt(1-4.*aX.*bXmm)/2./aX);%[m^-1]
kmaxmm = abs(1+sqrt(1-4.*aX.*bXmm)/2./aX);%[m^-1]
%kmaxmm=abs(qphon/2+m_eX*m_0*(hbar*(nu_s*qphon+omega_pt(indb))))...
%    /(hbar^2*qphon);%*****
expmm=exp(-eta+epsq+epspt);%[dimensionless]
expeminmm=exp(-hbar^2*kminmm.^2/(2*m_eGam*kB*Tc));%[-] assmd m_eGam
expemaxmm=exp(-hbar^2*kmaxmm.^2/(2*m_eGam*kB*Tc));%[-] assmd m_eGam
%    expemaxmm=0;%*****
logmm=log((expmm+expeminmm).*(exp(-eta)+exp(expemaxmm)))/...
((expmm+expemaxmm).*(exp(-eta)+exp(expeminmm))))...
./(exp(-epsq-epspt)-1);%[-] checked 8/2/07

```

```

%           logmp=0;%*****for debugging
%           logpm=0;%*****for debugging
%           logmm=0;%*****for debugging

%Nq=1/(exp(hbar*nu_s*qphon/(kB*Tc))-1);%found it! 8/4/07
Nq=1./(hbar*nu_s*qphon/(kB*Tc));%[dimensionless] approx above
logterm=- (Nq+1)/(exp(epsq+epspt)-1)*logpp...
          -(Nq)/(exp(-epsq+epspt)-1)*logmp...
          +(Nq+1)/(exp(epsq-epspt)-1)*logpm...
          +(Nq)/(exp(-epsq-epspt)-1)*logmm;%big fix 8/2/07
integrand1= qpnstep*qphon.^3*(MqsqGamL+MqsqGamX)*Vpn.*logterm;
              %[J^2*m^-1] chg, fixed 8/11/07
preHptcpn(inda,indb)=sum(integrand1);%[J^2*m^-1]*****
%tmpdata= [tmpdata integrand1];%for debugging*****
%       end
Hptcpn(inda,indb)=alphaconst*preHptcpn(inda,indb)/omega_pt(indb)^3;
              %[s^-1]
end
end

fprintf('\n')

%ptcarrint=zeros(length(matrix1),length(carrierstate));%*****for debugging
ptcarrint=Hptcpn*tstep2;%[s/s]
%matrix(t+\Delta{t})=(1-Rate*\Delta{t})*matrix(t)
%carrdecay=sum(pcd');%*****
carrdecay=sum(ptcarrint,2);%***** 2 is like '
carrcarrint=eye(length(carrierstate),length(carrierstate));
%carrcarrint=diag(exp(-tstep2./carrdecay));
%carrier-carrier interaction is negligible for intrinsic qty of carriers
A1 = [eye(length(matrix1),length(matrix1))*exp(-tstep2/tau),ptcarrint'];
%exp term accounts for losses that fall outside the EM window
%A1 = [eye(length(matrix1),length(matrix1)),ptcarrint'];
A2 = [ptcarrint,carrcarrint];
Aref = eye(length(matrix1),length(matrix1))*exp(-tstep2/tau);
% B matrix contains carrier state transition (carrier-photon) probs
%(Energy domain)

%format:
%B1=
%[(Identity      (photon-   ]
%[ Matrix)      carrier    ]
%[              coeffs)   ]

```

```

%%%%%%%%%%%%%%%%%%%%%%%%%%%%%%%%%%%%%%%%%%%%%%%%%%%%%%%%%%%%%%%%%%%%%%%%%% [
%B2=
%[(photon-      (carrier  )%should there be carrier-phonon?*****
%[carrier      decays)   ]
%[ coeffs)      ]

B1 = [eye(length(omega_pt),length(omega_pt)) -pcd' ];
B2= [-pcd, carrcarrint];
%B2= [pcd diag(exp(-tstep2./carrdecay))];
matrixref=matrix;
for em = 1:length(t2)
%4 step process:
%1.) use electron state and photon state to generate new photon
% state from field-carrier-phonon interaction
%2.) use electron state and photon state to generate new carrier state from
% field-carrier-phonon interaction
%3.) use electron state and photon state to generate new photon state from
% free-carrier emission
%4.) use electron state and photon state to generate new carrier state from
% free-carrier emission

encarry=encarry+1;%used to plot all the 3 parts of the graph on same screen
% %      peak= exp(-t2(em)/tau);
% %      width= width0/exp(-t2(em)/tau2);
% %      pk1= peak/(squeeze)^(.25);
matrixref(:,encarry)=Aref*matrixref(:,(encarry-1));
matrix(:,encarry)=matrix1;
carrmat(:,encarry)=carrierst1;
%matrix1=A*matrix1;
matrix1=A1*[matrix1;carrierst1];
%carrierst1=A2*[matrix1;carrierst1];%*****commented assumes field
%*****has little effect on carr)
%matrix1=B1*[matrix1;carrierstate];
%carrierstate=B2*[matrix1;carrierstate];%future work eventually should
%be uncommented*****
%%pk1*(exp(-((X-(cf+fplus*squeeze-shift)).^2)/(2*(width*squeeze)^2))...
% %      +exp(-((X-(cf+fminus*squeeze-shift)).^2)/(2*(width*squeeze)^2)));
% %
end
t3 = (t23jnt+0.001e-8):.3e-11:(t23jnt+0.1e-8);
%old expansion method no longer works:
%t3 = 1e-8:.3e-11:1.1e-8;original
% for owe=1:length(t3)
%      peak= exp(-t3(em)/tau);

```

```

%   encarry = encarry+1;
%   shift =-atan((t3(owe)-.5*n-t3(1))/shiftfactor)/pi*delcf+.5*delcf;
%   %shift = t(en)/n*.01;
%   squeeze=.5+atan((t3(owe)-t3(1)-.5*n)/squeezefactor)/pi;
%   pk1= peak/(squeeze)^(.25);
%   matrix(:,encarry)=pk1*(exp(-((X-(cf+fplus*squeeze-shift)).^2)/...
%       (2*(width*squeeze)^2))...
%       +exp(-((X-(cf+fminus*squeeze-shift)).^2)/(2*(width*squeeze)^2)));
% end

figure(6)
surf(carrmat);shading flat
% offset=max(matrix(:,length(matrix(1,:))))-...
%   max(matrixref(:,length(matrix(1,:)))));
offset=max(matrix(:,encarry))-max(matrixref(:,encarry));
T=[t t2 t3];
figure(7)
imagesc((0:1/(length(T)-1):1),X,abs(matrix).^(.625))%exponent scale factor
%to scale brightness
axis([0 1 0.9999999*min([f1 f2 cff-fplus cff-fminus])...
      1.0000001*max([f1 f2 cff-fplus cff-fminus])])
%axis([0 max(max(matrix)) 0.9999999*min([f1 f2 cff-fplus cff-fminus])...
%      1.0000001*max([f1 f2 cff-fplus cff-fminus])])

colormap([0:255; [0:.1:13.4 13.6:1.5:130*1.5];...
          [0:.1:13.4 13.6:1.5:130*1.5]'/255)

ylabel('Frequency, [ $\omega/2\pi$ ]')
ylabel('Frequency, [THz]')

TTickstep=floor(length(T)/7);
%TTicks= [0 1:3:20 21];
TTicks= T(1:TTickstep:length(T))/n;
XTicks= X(1:floor(length(X)/10):length(X));
set(gca,'XTick',0:1/11:1)
set(gca,'XTickLabel',...
      num2str(1e9*T(1:floor(length(T)/11):(length(T))),'.1f'))
%set(gca,'XTickLabel',num2str([0 .5 1 5.5 10 10.5 11]','.1f'))
%mxs=max(get(gca,'YTick'));
set(gca,'YTick',XTicks)
%set(gca,'YTickLabel',num2str(XTicks, '.8f'))
set(gca,'YTickLabel',num2str(1e-12*c/a*XTicks, '.5f'))
xlabel('Time, [ns]')

```

```

figure(8)
%plot(t, atan((t-.5*n)/n*100)/2/pi*delcf+.5*delcf)
plot(X,[matrix(:,entoo+1) matrix(:,end)-offset])%*[1 0;0 30])
xlim([X(min(find(matrix(:,entoo+1)>eps)))...
      X(max(find(matrix(:,entoo+1)>eps)))]])
ylim([min(min(matrix)) 1.5*max(max(matrix))])
limsx = get(gca,'XLim');
xlimv = limsx(1):diff(limsx)/4:limsx(2);
set(gca,'XTick',xlimv)
%set(gca,'XTick',XTicks)
%set(gca,'XTickLabel',num2str(xlimv','%.8f'))
set(gca,'XTickLabel',num2str(1e-12*c/a*xlimv','%.6f'))
xlabel('Frequency, [\omegaa/2\pic]')
ylabel('Amplitude, (Normalized)')
%figure(4)
%plot(t, atan((t-.5*n)/n*5)/pi+.5)
figure(9)

plot(X,abs((matrix(:,length(matrix(1,:)))-offset)./...
  matrixref(:,length(matrix(1,:))-1)*100)%*[1 0;0 30])
xlim([X(min(find(matrix(:,entoo+1)>eps)))...
      X(max(find(matrix(:,entoo+1)>eps)))]])
ylim([0 5])
limsx = get(gca,'XLim');
xlimv = limsx(1):diff(limsx)/4:limsx(2);
set(gca,'XTick',xlimv)
%set(gca,'XTick',XTicks)
set(gca,'XTickLabel',num2str(xlimv','%.8f'))
xlabel('Frequency, [\omegaa/2\pic]')
ylabel('Percent Difference in Amplitude')
title('Change Introduced by Considering Thermal Effect')

figure(5)%sanity check figure for photon-phonon coupling coeffs
surf(omega_pt,elecenergies,Hptcpn)
shading flat

%sanity check figures:photon-carrier
figure(1);plot(sum(Hcpt'));shading flat
figure(2);surf(omega_pt,elecenergies,Hcpt);shading flat

figure(3);plot(elecenergies/ec,carrierstate/estep*ec)
xlabel('Energy, [eV]')
ylabel('Carrier Distribution [carriers/eV/m^3]')

```

```
%title('Carrier Distribution')  
figure(4);surf(Hptcpn);shading flat
```



```

(material (make dielectric (epsilon 11.999))))))

(set! geometry (append geometry
  (list (make cylinder (center -3 6 0)
    (radius 0.2) (height infinity)
    (material (make dielectric (epsilon 1)))))))
(set! geometry (append geometry
  (list (make cylinder (center -3 6 0)
    (radius 0.1) (height infinity)
    (material (make dielectric (epsilon 11.999)))))))

(set! geometry (append geometry
  (list (make cylinder (center -3 14 0)
    (radius 0.2) (height infinity)
    (material (make dielectric (epsilon 1)))))))
(set! geometry (append geometry
  (list (make cylinder (center -3 14 0)
    (radius 0.1) (height infinity)
    (material (make dielectric (epsilon 12.001)))))))

(set! geometry (append geometry
  (list (make cylinder (center 3 -6 0)
    (radius 0.2) (height infinity)
    (material (make dielectric (epsilon 1)))))))

(set! geometry (append geometry
  (list (make cylinder (center 3 -6 0)
    (radius 0.1) (height infinity)
    (material (make dielectric (epsilon 11.999)))))))

(set! geometry (append geometry
  (list (make cylinder (center 3 -14 0)
    (radius 0.2) (height infinity)
    (material (make dielectric (epsilon 1)))))))

(set! geometry (append geometry
  (list (make cylinder (center 3 -14 0)
    (radius 0.1) (height infinity)
    (material (make dielectric (epsilon 12.001)))))))

(set! k-points (list ; create Brillouin zone
  (vector3 0 0 0) ; Gamma
  (vector3 .5 0 0) ; X
  ));(vector3 .5 .5 0) ; M

```

```
;(vector3 0 0 0)) ; Gamma

(set! k-points (interpolate 4 k-points)) ;interpolate along edge

(set! resolution 8)
(set! target-freq (/ (+ 0.2812 0.4174) 2))
(set! tolerance 1e-8)

;(include "dos.scm")
;(print-dos 0 1 100)

;(run-tm)
(run-tm (output-at-kpoint (vector3 0.5 0 0) output-efield-z))
;(output-efield-z 190)
;(output-efield-z 191)
;(output-efield-z 192)
;(output-efield-z 193)
;(output-efield-z 194)
```

Bibliography

- [1] ABRAM, I. Quantum theory of light propagation: Linear medium. *Phys. Rev. A* 35, 11 (June 1987), 4661–4672.
- [2] AFSAR, M. N., CHI, H., AND LI, X. Millimeter wave complex refractive index, complete dielectric permittivity and loss tangent of high purity and compensated silicon. *IEEE Conference on Precision Electromagnetic Measurements, 1990. CPEM '90 Digest.* (June 1990), 238–239.
- [3] BLAKEMORE, J. S. Semiconducting and other major properties of gallium arsenide. *Journal of Applied Physics* 53, 10 (Oct. 1982), R123–R181.
- [4] COHEN-TANNOUJJI, C., DIU, B., AND LALOË, F. *Quantum Mechanics*, vol. II. John Wiley and Sons, 1977.
- [5] CORNELIUS, C. M., AND DOWLING, J. P. Modification of planck blackbody radiation by photonic band-gap structures. *Phys. Rev. A* 59, 6 (June 1999), 4736–4746.
- [6] DAVIS, P. W. *Differential Equations for Mathematics, Science, and Engineering.* Prentice Hall, 1992.
- [7] ELISEEV, P. G., DRAKIN, A. E., AND PITTROFF, W. A study of laser emission wavelength variations in 1.5 μm ingaasp/inp brs laser diodes: Theoretical model and experiment. *IEEE J. of Quantum Electron.* 39, 9 (Sept. 2003), 1060–1065.
- [8] FLORESCU, M., LEE, H., STIMPSON, A. J., AND DOWLING, J. P. Thermal emission and absorption of radiation in finite inverted-opal photonic crystals. *Phys. Rev. A* 72 (Sept. 2005), 033821.

- [9] FRONEN, R. J., AND VANDAMME, L. K. J. Low-frequency intensity noise in semiconductor lasers. *IEEE J. of Quantum Electron.* 24, 5 (May 1988), 724–736.
- [10] GILES, F. P., SANII, F., SCHWARTZ, R. J., AND GRAY, J. L. Nondestructive contactless measurement of bulk lifetime and surface recombination using single pass infrared free carrier absorption. *Conference Record of the Twenty Second IEEE Photovoltaic Specialists Conference, 1991.* (Oct. 1991), 223–228.
- [11] GORODETSKY, M. L., AND ILCHENKO, V. S. High-Q optical whispering-gallery microresonators: precession approach for spherical mode analysis and emission patterns with prism couplers. *Optics Communications* 113 (Dec. 1994), 133–143.
- [12] GRIFFITHS, D. *Introduction to Quantum Mechanics.* Prentice Hall, Inc., 1995.
- [13] JIANG, H., HINCKNEY, J. M., AND SINGH, J. Carrier dynamics studies through free-carrier absorption: A monte carlo study for silicon. *IEEE J. of Quantum Electron.* 33, 10 (Oct. 1997), 1779–1783.
- [14] JOANNOPOULOS, J., MEADE, R. D., AND WINN, J. N. *Photonic Crystals: Molding the Flow of Light.* Princeton University Press, 1995.
- [15] JOHNSON, S. G., AND JOANNOPOULOS, J. D. Block-iterative frequency-domain methods for maxwell’s equations in a planewave basis. *Optics Express* 8, 3 (Jan. 2001), 173–190.
- [16] KIM, K.-Y., LEE, B., AND LEE, C. Modeling of interband and free-carrier absorption coefficient in heavily doped conduction-band quantum-well structures. *IEEE J. of Quantum Electron.* 35, 10 (Oct. 1999), 1491–1501.
- [17] LAU, F. K., TEE, C. W., PENTY, R. V., WHITE, I. H., MICHAEL, N., AND KRAKOWSKI, M. A novel intracavity lens design for compact and high efficiency tapered laser diode. *IEEE Photonics Technology Letters* 19, 4 (Feb. 2007), 203–205.
- [18] MILONNI, P. W. Why spontaneous emission. *Am. J. Phys.* 52, 4 (Apr. 1984), 340–343.

- [19] PIERRET, R. F. *Semiconductor Device Fundamentals*. Addison-Wesley Publishing Company, 1996.
- [20] POZAR, D. M. *Microwave Engineering*. John Wiley and Sons, 2005.
- [21] SAKODA, K. *Optical Properties of Photonic Crystals*. Springer-Verlag, 2001.
- [22] SALEH, B., AND TEICH, M. *Fundamentals of Photonics*. John Wiley and Sons, 1991.
- [23] SANDROCK, M., WIGGINS, M., SHIRK, J. S., TAI, H., RANADE, A., BAER, E., AND HILTNER, A. A widely tunable refractive index in a nanolayered photonic material. *Appl. Phys. Lett.* 84, 18 (May 2004).
- [24] SCHRODER, D. K., THOMAS, R. N., AND SWARTZ, J. C. Free-carrier absorption in silicon. *IEEE J. of Solid-State Circuits* SC-13, 1 (Feb. 1978), 180–187.
- [25] SCULLY, M. O., AND ZUBAIRY, S. *Quantum Optics*. Cambridge University Press, 1997.
- [26] SPITZER, W. G., AND WHELAN, J. M. Infrared absorption and electron effective mass in *n*-type gallium arsenide. *Phys. Rev.* 114, 1 (Apr. 1959), 59–63.
- [27] SPRIK, R., TIGGELEN, B. V., AND LAGENDIJK, A. Optical emission in periodic dielectrics. *Europhys. Lett.* 35, 4 (Aug. 1996), 265–270.
- [28] TATAKI, K., KISE, T., MARUYAMA, K., YAMANAKA, N., FUNABASHI, M., AND KASUKAWA, A. Reduced linewidth re-broadening by suppressing longitudinal spatial hole burning in high-power 1.55- μm continuous-wave distributed-feedback (cw-dfb) laser diodes. *IEEE J. of Quantum Electron.* 39, 9 (Sept. 2003), 1060–1065.
- [29] THOMPSON, M. *Intuitive Analog Circuit Design*. Elsevier (Newnes), 2006.
- [30] TIEDJE, T., YABLONOVITCH, E., CODY, G. D., AND BROOKS, B. G. Limiting efficiency of silicon solar cells. *IEEE Trans. Electron Devices* ED-31, 5 (May 1984), 711–716.

- [31] TSAI, C.-Y., TSAI, C.-Y., CHEN, C.-H., SUNG, T.-L., WU, T.-Y., AND SHIH, F.-P. Theoretical model for intravalley and intervalley free-carrier absorption in semiconductor lasers: Beyond the classical drude model. *IEEE J. of Quantum Electron.* *34*, 3 (Mar. 1998), 552–559.
- [32] VAINOS, N. A., KHOURY, J. A., AND EASON, R. W. Real-time parallel optical logic in photorefractive bismuth silicon oxide. *Opt. Lett.* *13*, 6 (June 1988), 503–505.
- [33] WILLATZEN, M., USKOV, A., MØRK, J., TROMBORG, B., AND JAUHO, A.-P. Non-linear gain suppression in semiconductor lasers due to carrier heating. *IEEE Photonics Technology Letters* *3*, 7 (July 1991), 606–609.
- [34] YANG, S. Y., CHIEH, J. J., HORNG, H. E., HONG, C.-Y., AND YANG, H. C. Origin and applications of magnetically tunable refractive index of magnetic fluid films. *Appl. Phys. Lett.* *84*, 25 (June 2004), 5204–5206.
- [35] YANIK, M. F., AND FAN, S. Stopping light all optically. *Phys. Rev. Lett.* *92*, 8 (Feb. 2004), 083901.
- [36] YANIK, M. F., FAN, S., SOLJACIC, M., AND JOANNOPOULOS, J. All-optical transistor action with bistable switching in a photonic crystal cross-waveguide geometry. *Opt. Lett.* *28*, 24 (Dec. 2003), 2506–2508.
- [37] YARIV, A., XU, Y., LEE, R. K., AND SCHERER, A. Coupled-resonator optical waveguide: a proposal and analysis. *Opt. Lett.* *24*, 11 (June 1999), 711–713.
- [38] ZHU, Z.-H., YE, W.-M., JI, J.-R., YUAN, X.-D., AND ZEN, C. High-contrast light-by-light switching and and gate based on nonlinear photonic crystals. *Optics Express* *14*, 5 (Mar. 2006), 1784.